www.coinweb.no

SINTEF Building and Infrastructure Håvard Nedrelid (NTNU)

Structural FRC – Design approach and experimental results

COIN project report 66 – 2015

SINTEF

SINTEF Building and Infrastructure

Håvard Nedrelid (NTNU)

Structural FRC – Design approach and experimental results

FA 2 Competitive construction

SP 2.2 Ductile high tensile strength concrete

COIN Project report 66 – 2015

COIN Project report no 66
Håvard Nedrelid (NTNU)
Structural FRC – Design approach and experimental results
FA 2 Competitive construction
SP 2.2 Ductile high tensile strength concrete

Keywords:
FRC, fibre

Project no.: 102000442-4

ISSN 1891–1978 (online)
ISBN 978-82-536-1466-3 (pdf)

Address: Forskningsveien 3 B
POBox 124 Blindern
N-0314 OSLO
Tel: +47 73 59 30 00
Fax: +47 22 69 94 38

www.sintef.no/byggforsk
www.coinweb.no

Cooperation partners / Consortium Concrete Innovation Centre (COIN)

Kværner Engineering
Contact: Jan-Diederik Advocaat
Email: Jan-Diederik.Advocaat@kvaerner.com
Tel: +47 67595050

Saint Gobain Weber
Contact: Geir Norden
Email: geir.norden@saint-gobain.com
Tel: +47 22887700

Norcem AS
Contact: Terje Rønning
Email: terje.ronning@norcem.no
Tel: +47 35572000

NTNU
Contact: Terje Kanstad
Email: terje.kanstad@ntnu.no
Tel: +47 73594700

Mapei AS
Contact: Trond Hagerud
Email: trond.hagerud@mapei.no
Tel: +47 69972000

SINTEF Building and Infrastructure
Contact: Tor Arne Hammer
Email: tor.hammer@sintef.no
Tel: +47 73596856

Skanska Norge AS
Contact: Sverre Smeplass
Email: sverre.smeplass@skanska.no
Tel: +47 40013660

Norwegian Public Roads Administration
Contact: Kjersti K. Dunham
Email: kjersti.kvalheim.dunham@vegvesen.no
Tel: +47 22073940

Unicon AS
Contact: Stein Tosterud
Email: stto@unicon.no
Tel: +47 22309035

Veidekke Entreprenør ASA
Contact: Christine Hauck
Email: christine.hauck@veidekke.no
Tel: +47 21055000

Contents

1 General introduction

Fibre-reinforced concrete (FRC) may be defined as concrete containing relatively short, discrete, discontinuous fibres. Even at low fibre contents, the addition of fibres significantly increases the post-cracking toughness and ductility of the concrete[1]. Another benefit of fibres is reduced crack width and spacing. The fibres tend to bridge the cracks and thereby control the crack development and prevent the occurrence of large crack widths. The tensile strength may also be increased, but a high volume percentage of fibres are then required to get any substantial increase.

The enhanced post-cracking tensile behaviour and improved crack control of concrete may lead to significant improvements in the behaviour of the resulting structural members, both at the serviceability-limit state (SLS) and at the ultimate-limit state (ULS). Use of FRC for structural applications therefore holds the potential for reducing or even eliminating the conventional bar reinforcement, which in turn may lessen the congestion of reinforcement and lead to more efficient designs.

However, fibres are currently only used for structural parts where reinforcement is not statically required, e.g. in walls and slabs on grade where only a minimum amount of reinforcement is needed for crack control. Nonetheless, a vision in COIN is that fibres, one day in the future, will be able to fully or partially replace the conventional steel bars in structural members [1]. However, in order to reach this goal, there is still need for more experimental research in order to verify and, if necessary, modify, the tentative design rules published as 'COIN project report 29' [2].

The aim of this report is to briefly review the background for the COIN design approach and further evaluate it against experimental data. The data stems from two test programs conducted at NTNU as part of the master's theses written by Nordhus, Steinnes and Simpson; and Backe-Hansen and Hamstad during spring 2011.

In the former test program [3], the main scope was to examine if the COIN approach for the calculation of crack widths, moment resistance and shear resistance can be used to predict the behaviour of RC bending members made of ductile self-compacting FRC. In this respect, a multi-layer beam model was used to simulate the bending behaviour and to estimate the compressive depth of the concrete and the stress in the flexural bars needed in the crack width calculations.

In the latter test program [4], the possibility of simplifying the detailing of dapped beam ends by the use of fibres was investigated. In this respect, the performance of dapped end RC beams made of ductile self-compacting FRC, with simplified reinforcement layout, was compared to that a conventionally dapped end RC beam of ordinary concrete. The structural behaviour of the dapped ends was further compared to the COIN design rules and a strut-and-tie model (STM) was suggested.

[1] Toughness can be defined as the energy absorption capacity of the material and is related to the area under the stress-strain curve. Ductility can be defined as the ability of the material to deform inelastically without loss of load-carrying capacity.

2 The COIN design approach

2.1 Basic concept

Within manageable fibre contents for ordinary cast concrete, i.e. up to about 2.0 vol% [5], it is assumed that only the tensile properties of the concrete are altered by the inclusion of fibres. Since it is mostly the post-cracking behaviour that is affected, the characteristic residual tensile strength at $2.5\,mm$ crack width is chosen as the material parameter governing the effect of fibres. Hence, the compressive behaviour of structural FRC can be expressed in terms of the characteristic cylinder compressive strength, f_{ck}, in the same manner as for ordinary concrete [6], while the tensile behaviour is deemed to be fully described by the characteristic residual tensile strength at $2.5\,mm$. Its value is derived from the flexural tensile strength at $2.5\,mm$ crack width, $f_{R,3}$, established from flexural tests executed at 28 days on notched prisms according to EN 14651 [7].

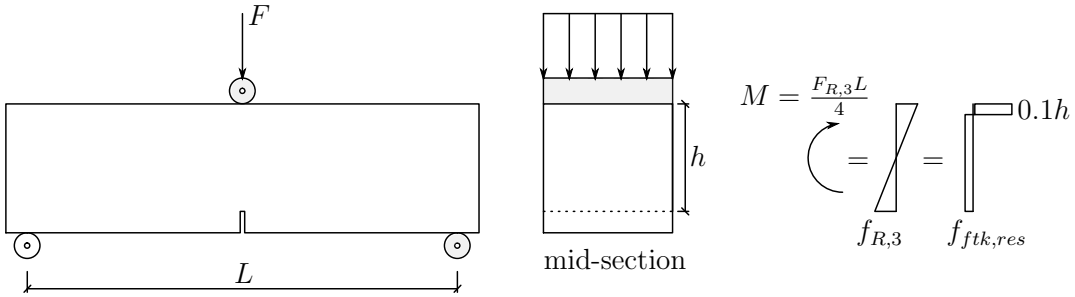

Figure 1: Test set-up for measuring the residual flexural strength of FRC according to EN 14651, together with the assumed relationship between the characteristic residual flexural strength and the characteristic residual tensile strength.

In the EN 14651 tests, a load is applied through a steel roller to a $150 \times 150 \times 550\,mm$ notched prism spanning $500\,mm$ between two steel rollers, as shown in figure 1. From the applied load and the measured deflection at mid-span, the corresponding load/CMOD[2]-diagram can be deduced. This allows the flexural strength at a given crack-width to be established. Its characteristic value (5 % fractile of distribution) is further translated into a characteristic residual tensile strength by equating the moments from the two stress distributions in figure 1, which yields the expression

$$f_{Rk,3} \cdot \frac{bh^2}{6} = f_{ftk,res,2.5} \cdot b \cdot 0.9h \cdot 0.5h \tag{1}$$

from which the following simple translation formula is derived

$$f_{ftk,res,2.5} = 0.37 f_{Rk,3} \tag{2}$$

However, if the fibre orientation and the fibre content in the EN 14651 test specimens is not considered to be representative for the casting conditions in the actual structural

[2]Crack mouth opening displacement

member, the residual tensile strength should be normalised through the equation

$$f_{ftk,res,2.5,norm} = \frac{f_{ftk,res,2.5} \cdot \nu_{f,nom}}{\nu_f(4\alpha - 1)} \tag{3}$$

where

$\nu_{f,nom}$ = nominal fibre content according to mix design
ν_f = actual fibre content in the EN 14651 prisms
α = actual fibre orientation factor in the EN 14651 prisms

Moreover, if the fibre orientation factor in the structural member is documented and is not isotropic (i.e. is not 0.5), the residual tensile strength may be corrected through the following expression

$$f_{ftk,res,2.5,struct} = f_{ftk,res,2.5,norm} \frac{(4\alpha_{struct} - 1)\nu_{f,struct}}{\nu_{f,nom}} \tag{4}$$

where

$\nu_{f,nom}$ = nominal fibre content according to mix design
$\nu_{f,struct}$ = actual fibre content in the structural member
α_{struct} = actual fibre orientation factor in the structural member

2.2 Design rule proposals

2.2.1 Moment resistance

The moment resistance of reinforced FRC cross-sections can be calculated as for ordinary concrete in EC2 clause 6.1(2)P, but with an additional rectangular tensile stress block equal to the design value of the characteristic residual tensile strength. Equilibrium of

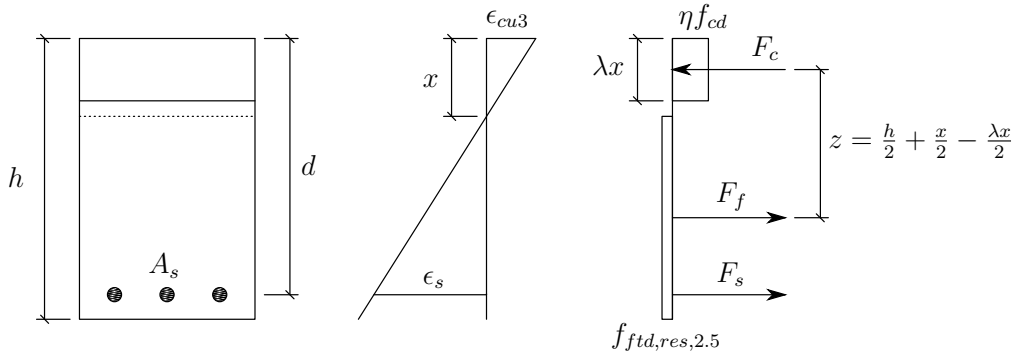

Figure 2: Stress and strain distribution for a rectangular cross-section of reinforced FRC in pure bending at the ultimate-limit state.

moment about the compression resultant yields the following expression for the moment resistance

$$M_{Rd} = \overbrace{Asf_{yd}}^{F_s}(d - \tfrac{\lambda x}{2}) + \overbrace{b(h-x)f_{ftd,res,2.5}}^{F_f}(\tfrac{h}{2} + \tfrac{x}{2} - \tfrac{\lambda x}{2}) \tag{5}$$

If the maximum tensile strain exceeds 3/h (where h is given in mm), the compressive strain and the maximum tensile strain is set equal to ϵ_{cu3} and $3/h$ respectively.

2.2.2 Shear resistance

The shear resistance of reinforced FRC cross-sections can be calculated as for ordinary concrete in EC2 clause 6.2.2(1), but with an additional fibre contribution term. The total resistance is then given by

$$V_{Rd,c} = V_{Rd,ct} + V_{Rd,cf} \tag{6}$$

where the first term on the right-hand side is the design value for the shear resistance in EC2 given as

$$V_{Rd,ct} = [C_{Rd,c}k(100\rho_l f_{ck})^{1/3} + k_1\sigma_{cp}]b_w d >= (\nu_{min} + k_1\sigma_{cp})b_w d \tag{7}$$

while the latter term accounts for the effect of fibres through the following simple expression

$$V_{Rd,cf} = 0.6f_{ftd,res,2.5}b_w h \tag{8}$$

2.2.3 Calculation of crack widths

According to clause 7.3.4 in EC2, the characteristic crack width is given by

$$w_k = s_{r,max}(\epsilon_{sm} - \epsilon_{cm}) \tag{9}$$

The strain difference in this expression can be calculated as for ordinary concrete. However, as will be shown in the following, a new coefficient needs to be introduced in the crack spacing formula.

If it is assumed that no crack can form within s_0 of an existing crack, this defines the minimum crack spacing. The maximum crack spacing is then $2s_0$, since if a wider spacing existed a new crack could form. Hence, if it is assumed that the bond stress is constant along the length s_0 and that the stress, due to the build-up of stresses transferred from the reinforcement to the concrete through bond, will just reach the tensile strength of the concrete at a distance s_0 from a crack, then

$$\tau\pi\phi s_0 + A_c f_{ftk,res,2.5} = A_c f_{ctm}$$

where τ is the bond stress, A_c is the area of the concrete, f_{ctm}, is the tensile strength of the concrete and ϕ is the bar diameter. By taking $\rho = \pi\phi^2/4A_c$ and substituting for A_c the following expression is obtained

$$s_0 = \frac{1}{4} \cdot \frac{(f_{ctm} - f_{ftk,res,2.5})}{\tau} \cdot \frac{\phi}{\rho_s}$$

The average crack spacing can be taken as the mean of s_0 and $2s_0$, which yields

$$s_m = \frac{3}{8} \cdot \frac{(f_{ctm} - f_{ftk,res,2.5})}{\tau} \cdot \frac{\phi}{\rho_s}$$

Further, experimental investigations have shown that the average bond stress may be estimated as

$$\tau = \frac{3}{2 \cdot k_1} \cdot f_{ctm}$$

By substituting this relation into the above crack spacing formula, the expression becomes

$$s_m = 0.25 \cdot k_1 \overbrace{\left(1 - \frac{f_{tk,res,2.5}}{f_{ctm}}\right)}^{k_5} \frac{\phi}{\rho_s}$$

This is similar to the most primitive relationship for the prediction of crack spacings, but with an additional coefficient which accounts for the effect of fibres. However, as for ordinary concrete, in order to be able to apply it to bending, a coefficient k_2 is introduced and an effective reinforcement ratio $\rho_{p,eff}$ must be defined. Moreover, since experimental studies have shown that the cover also has a significant influence on crack spacings, an extra term $2c$ is introduced where c is the cover to the longitudinal reinforcement. The expression for the average crack spacing may then be rewritten as

$$s_{r,m} = 2c + 0.25 k_1 k_2 k_5 \frac{\phi}{\rho_{p,eff}}$$

where k_5 is the additional factor which accounts for the effect of fibres. However, in design, it is not the average crack width which is required, but a value that is unlikely to be exceeded. A reasonable estimate of the characteristic width (with 5 % probability of being exceeded) is obtained if the maximum crack spacing is assumed to be 1.7 times the average value. This leads to the following expression for the maximum final crack spacing

$$s_{r,max} = k_3 c + k_1 k_2 k_4 k_5 \frac{\phi}{\rho_{p,eff}} \tag{10}$$

where

k_1 = coefficient for bond properties of reinforcement (0.8 for full bond)

k_2 = coeficient for distribution of strain (0.5 for bending)

k_3 = factor equal to 3.4

k_4 = factor equal to 0.425

k_5 = coefficient for the effect of fibres

This expression is similar to that given in EC2 clause 7.3.4(3), but with an additional factor, k_5, which accounts for the effect of fibres.

2.3 Multi-layer models

Hordijk developed a multi-layer model to study the response of plain concrete beams in bending [8]. However, the model can also be used to study the flexural response of reinforced FRC beams [9]. The basic principle is that two halves of a bending member are connected by springs which represents the behaviour of small layers. A linear strain distribution over the height of the cross-section is further assumed. Hence, when the material behaviour of the reinforcement and the concrete is known, the response of the beam can be taken as the sum of the behaviour of all springs, given that equilibrium is fulfilled. Equilibrium is satisfied when the sum of horizontal internal forces is nearly zero, i.e. when

$$N = \sum_{i=1}^{n} \sigma_{c,i} \cdot b \cdot \frac{h}{n} + \sigma_s A_s + \sigma'_s A'_s \approx 0 \tag{11}$$

where

n = number of layers
b = width of cross-section
h = height of cross-section
$\sigma_{c,i}$ = concrete stress in each layer
σ_s = stress in tensile reinforcement
σ'_s = stress in compressive reinforcement
A_s = area of tensile reinforcement
A'_s = area of compressive reinforcement

By multiplying the internal forces in each layer and in the reinforcement with the corresponding internal level arm, the internal moment can be found as

$$M = \sum_{i=1}^{n} \sigma_{c,i} \cdot b \cdot \frac{h}{n} \cdot z_{c,i} + \sigma_s A_s \cdot z_s + \sigma'_s A'_s \cdot z'_s \tag{12}$$

where

$z_{c,i}$ = distance from mid-height to centre of each layer
z_s = distance from mid-height to centroid of tensile reinforcement
z'_s = distance from mid-height to centroid of compressive reinforcement

The entire moment-curvature response of the beam can then be simulated by increasing the curvature in small steps and solving for equilibrium of internal forces within each step. This can be done by keeping the strain in the bottom layer constant while the strain in the top layer is increased until the sum of horizontal internal forces is less than

a certain small value. Or, alternatively, by keeping the strain in the top layer constant while the strain in the bottom layer is increased until equilibrium is satisfied. If the former approach is adopted, the procedure within a step can be summarised as follows:

1. Determine the curvature from the strain in the top and bottom layer.
2. Calculate the corresponding strain in each layer and in the reinforcement.
3. Establish the corresponding stresses from the constitutive relations.
4. Find the internal forces and moments from Equation 11 and 12.
5. If the sum of internal forces are not nearly zero, increase the strain in the top layer and repeat the procedure.

The entire moment-curvature relationship of the beam can then be simulated by successively increasing the strain in the bottom layer.

This procedure is straightforward enough, but it relies on a realistic description of the material behaviour. For concrete in compression and the reinforcement, the relationships given in EC2 clause 3.1.7 and 3.2.7 can be used, whereas for the concrete in tension it can be assumed that the behaviour is linear elastic until the tensile strength is reached and the stress drops immediately to the residual tensile strength. Or, alternatively, if the residual tensile strength is larger than the direct tensile strength, the behaviour is assumed to be linear elastic until the residual tensile strength is reached. In both of these cases the residual tensile strength is assumed to follow a constant 'yield' plateau until the failure strain 3/h is reached.

3 Reinforced SC-HFRC members in bending

3.1 Introduction

Vibrating the concrete has a negative effect on the distribution and the orientation of fibres. Self-compacting concrete (SCC) is therefore likely to enhance the load-carrying capacity of FRC members due to the alignment of the fibres in the direction of flow. To further increase contribution of the fibres to the structural load-carrying capacity, it should be aimed for the highest possible concrete ductility. This may be achieved by using a combination of fibres, sometimes referred to as hybrid-fibre-reinforced concrete (HFRC). An experimental program was therefore undertaken to study the behaviour of reinforced SC-HFRC members in bending The main scope was to evaluate if the design approach for shear resistance, moment resistance and crack widths in 'COIN Project report 29' is applicable. This mainly involves checking if the residual tensile strength at $2.5\,mm$ crack width, as established from flexural tests on small notched prisms, can be used to predict the effect of fibres in the structural members.

3.2 Experimental program

3.2.1 Brief overview

A series of four reinforced SC-HFRC members were tested. Two types of SC-HFRC were included in the test program: one mix with 1.0 vol% steel fibres + 1.0 vol% synthetic fibres; and one mix with 0.5 vol% steel fibres + 0.5 vol% synthetic fibres. A flexural beam of each concrete type, and a one-way flexural slab and a shear beam of the latter, were loaded in four-point bending until failure. Each test was replicated one time, resulting in a total number of eight structural members.

3.2.2 Materials

Details of the mix design for the two SC-HFRCs are given in table 1. It can be seen that the effective water-cement ratio is about 0.66 and 0.79 for the two mixes respectively. Dramix 65/60 is a cold drawn steel wire fibre with hooked ends (length $l = 60\,mm$, aspect ratio $l/d = 67$, tensile strength $\sigma_t = 1000\,MPa$), whereas Barchip shogun is a synthetic polymeric fibre with embossed surface texture (length $l = 48\,mm$, tensile strength $\sigma_t = 550\,MPa$, Youngs modulus $E = 10\,GPa$). Moreover, two types of liquid admixtures were used, Dynamon SP-130 to increase the flowability and Viscostar 3K to control the viscosity. The dry content of these is about 30 % and 4 % respectively.

Table 1: Composition of the different concretes utilised in the test program. All components are specified by its dry content except for water.

Components in kg/m^3	SC-HFRC 2.0 vol%	SC-HFRC 1.0 vol%
Norcem standard cement	314	288
Limestone powder	78.5	71.9
Effective water	208	228
Årdal aggregate $(0-8\,mm)$	1468	1416
Årdal aggregate $(0-2\,mm)$	259	250
Dynamon SP-130	1.22	1.13
Viscostar 3K	0.06	0.05
Dramix 65/60	78.0	39.0
Barchip Shogun 48	9.10	4.55
Total weight	2416	2298

The mixing procedure was as follows: add the dry components and mix for 2 minutes; add water and the viscosity modifier and about half of the superplastisizer during mixing; mix for 4 minutes and then rest for 10 minutes until potential false set; add more of the superplastisizer during mixing based on a visual estimate of the mix consistency; measure the slump flow; if the desired slump is achieved the concrete is poured back and fibres are added during mixing; if not, more superplastisizer should be added before the fibres are included in the mix.

Two flexural beams were cast from one 2.0 vol% batch, whereas two flexural beams, two flexural slabs, and two shear beams were cast from four 1.0 vol% batches. Moreover six $100\,mm$ cubical specimens and three $150 \times 150 \times 550\,mm$ prisms were cast for each of the five batches in order to determine the material properties. It should be noted that for the 2.0 vol% batch, the slump was not checked before the fibres were added, which led to an exaggerated use of superplastisizer and the mix separated. This should be kept in mind when ealuating the results.

Table 2: Mean residual tensile strengths from tests according to EN 14651. It should be noted that the tests were conducted at various ages of the concrete. The slump flow was measured by filling a standard cone with concrete, with no compaction, and then lifting it up to determine the spread.

Batch nr.	w/c-ratio	Fibre content (vol%)	Slump flow (mm)	Test age (days)	Residual tensile strength (MPa)
1	0.66	2.0	770	29	3.3
2	0.79	1.0	650	33	1.9
3	0.79	1.0	590	33	2.1
4	0.79	1.0	560	20	1.5
5	0.79	1.0	590	34	1.6

Flexural tests of the notched $150 \times 150 \times 550\,mm$ prisms were performed according to

EN 14651. The mean residual tensile strengths established from the tests are presented in Table 2, while the corresponding load-deflection curves are given in Figure 3.

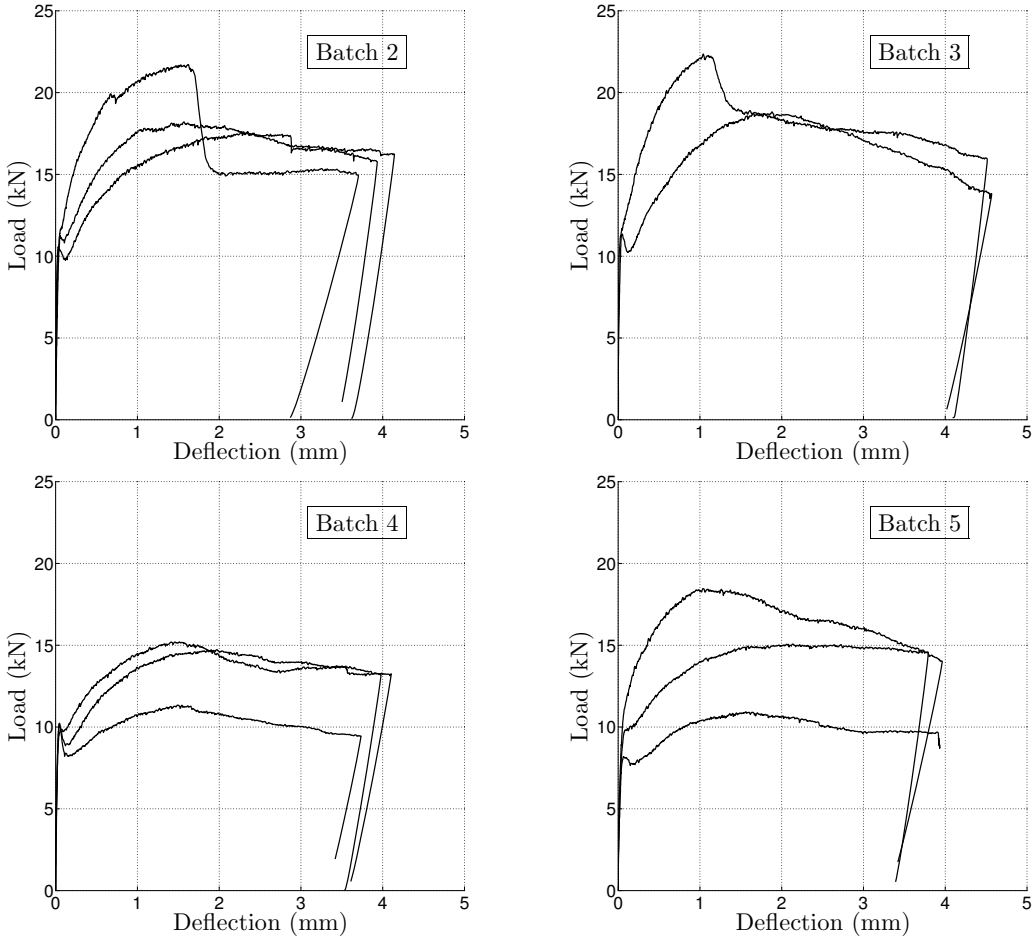

Figure 3: Load-deflection curves for the specimens from Batch 2 to 5. The cracking load can be recognised as the end of the nearly elastic part of the ascending branch of the curves. It can be seen that for all beams, the curves continue to rise after cracking. A long ascending part of the load-deflection curves after cracking is preferable, since this is synonymous with a high degree of ductility of the concrete.

3.2.3 Details of test specimens

Reinforced SC-HFRC beams designed for flexural failure. A simply-supported RC beam of each concrete type was loaded as shown in Figure 4. Each test was repeated one time, resulting in a total number of four specimens. The specimens were 200 mm wide, 300 mm deep and 4000 mm long with a span of 3000 mm. One 20 mm deformed bar with 45 mm cover (i.e. $d = 245\,mm$) was used as longitudinal tensile reinforcement. According to tensile tests, the yield stress of the steel bars was 566 MPa. The low amount of longitudinal tensile reinforcement ($\rho_l = 0.64\,\%$) together with the relatively high shear span-to depth ratio ($a/d = 4.1$) secured a flexural failure of all four specimens.

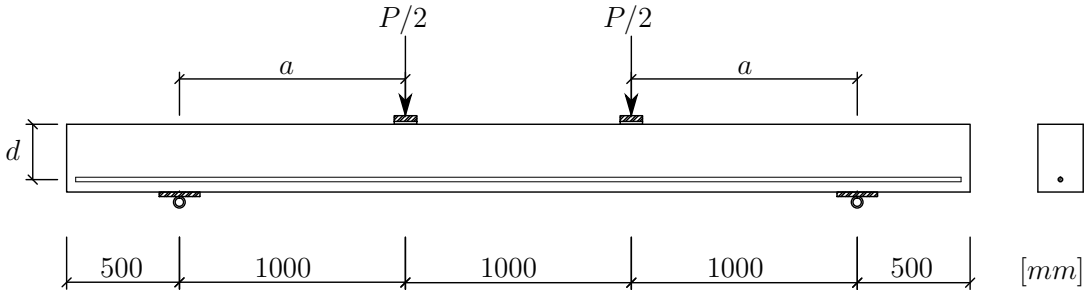

Figure 4: Test set-up and reinforcement layout for the four flexural beams. The left support is free to translate horizontally while the right support is pinned.

Reinforced SC-HFRC beam designed for shear failure. A simply-supported RC beam of the 1.0 vol%-mix was loaded as shown in Figure 12. Each test was repeated one time, resulting in a total number of two specimens. The specimens were 200 mm wide, 300 mm deep and 4000 mm long with a span of 3000 mm. Two centrally placed 32 mm deformed bars in two layers with 40 mm cover (i.e. $d = 228\,mm$) were used as longitudinal tensile reinforcement. In addition, a 25 mm deformed bar with 40 mm cover was used as compressive reinforcement. No stirrups were provided, except for two 8 mm stirrups at both ends for mounting purposes. The high amount of longitudinal tensile reinforcement ($\rho_l = 3.5\,\%$) combined with the relatively low shear span-to depth ratio ($a/d = 3.1$) led to a shear failure of both specimens.

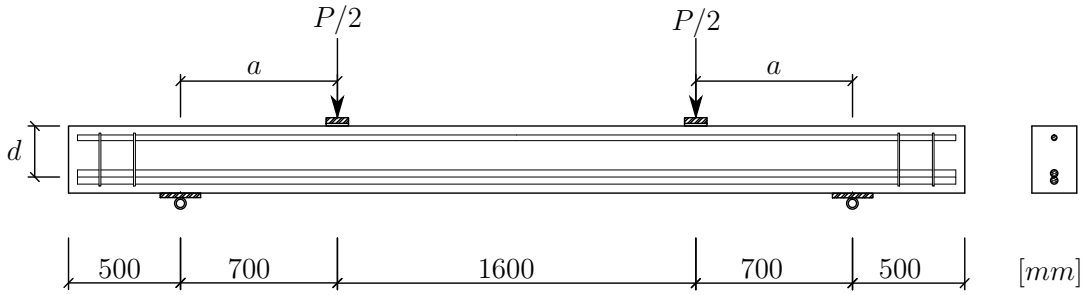

Figure 5: Test set-up and reinforcement layout for the two shear beams. The left support is free to translate horizontally while the right support is pinned.

Reinforced SC-HFRC slab designed for flexural failure. A simply-supported one-way RC slab of the 1.0 vol%-mix was loaded as shown in Figure 6. Each test was repeated one time, resulting in a total number of two specimens. The justification for the reverted loading arrangement is a more convenient monitoring of the crack development during testing. The specimens were 900 mm wide, 150 mm deep and 3000 mm long with a span of 900 mm. Two 8 mm deformed bars with 40 mm cover (i.e. $d = 106\,mm$) was used as longitudinal tensile reinforcement. The yield stress of the steel bars was assumed to be 500 MPa due to lack of experimental data. The low amount of longitudinal tensile reinforcement ($\rho_l = 0.10\,\%$) combined with the high shear span-to depth ratio ($a/d = 8.1$) secured a flexural failure of both specimens.

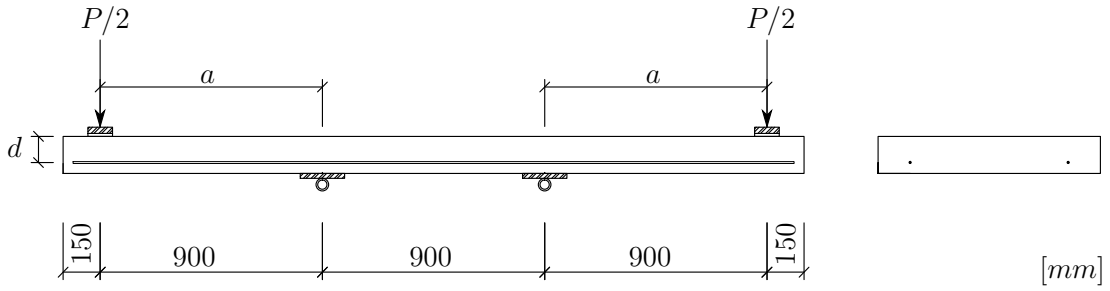

Figure 6: Test set-up and reinforcement layout for the two flexural slabs. The left support is free to translate horizontally while the right support is pinned.

3.2.4 Testing of specimens

The structural beam and slab specimens were loaded by a hydraulic jack with 1000 kN and 100 kN capacity, respectively. A steel profile was used to distribute the load from the jack to the loaded areas. The load was applied through a piece of plywood in order to ensure full contact over the entire loading area. The specimens rested onto steel plates which could freely rotate on top of a roller support at the left end and a pinned support at the other end. At mid-span, longitudinal strain gauges was mounted on each side in height of the tensile reinforcement and on the top surface of the compressive zone of the beams in order to monitor the curvature. Moreover, a LVDT was attached to the bottom face, which allowed the deflection at mid-span to be measured. For the slab specimens, one LVDT was attached to each corner and each side of the mid-span.

3.2.5 Relation between curvature and deflection

Since the strain readings for the flexural beams were unreliable and only deflections were measured for the slab specimens, the relation between curvature and deflection had to be established using the unit load method. The deflection may then be expressed through the curvature as

$$1 \cdot \delta = \int_0^L M' \cdot \frac{M}{EI}\,\mathrm{d}x = M' \cdot \kappa\,\mathrm{d}x \tag{13}$$

where M' and M is the variation of virtual and actual moment along the beam length and κ is the curvature corresponding to the actual moment. If it is assumed that the curvature is of the same shape as the moment diagram as shown in figure 7, the relationship becomes

$$\delta = \overbrace{2\int_0^{\frac{L}{3}} \frac{x}{2} \cdot \frac{3x}{L}\kappa \,\mathrm{d}x}^{\text{(A)+(D)}} + \overbrace{2\int_{\frac{L}{3}}^{\frac{L}{2}} \frac{x}{2} \cdot \kappa \,\mathrm{d}x}^{\text{(B)+(C)}} = \frac{1}{27}L^2\kappa + \frac{5}{72}L^2\kappa = \frac{23}{216}L^2\kappa \tag{14}$$

which yields the following simple translation formula

$$\kappa = \frac{216}{23} \cdot \frac{\delta}{L^2} \quad \forall \quad \delta \leq \delta_{peak} \tag{15}$$

This relation holds true until the peak load level is attained. After this stage, yielding of the flexural bars results in a larger curvature in the constant moment region and a smaller curvature in the shear spans. However, without too much error, it can be assumed that the curvature remains constant in the shear spans after peak (i.e. only the curvature in the constant moment region is assumed to increase with the deflection at mid-span after peak). The relation between deflection and curvature may then be written as

$$\delta = \frac{1}{27}L^2\left(\frac{216}{23} \cdot \frac{\delta_{peak}}{L^2}\right) + \frac{5}{72}L^2\kappa = \frac{8}{23}\delta_{peak} + \frac{5}{72}L^2\kappa \tag{16}$$

which, when rearranged, yields the following relation between the curvature and the deflection at mid-span

$$\kappa = \frac{72}{5} \cdot \frac{\delta - \frac{8}{23} \cdot \delta_{peak}}{L^2} \quad \forall \quad \delta > \delta_{peak} \tag{17}$$

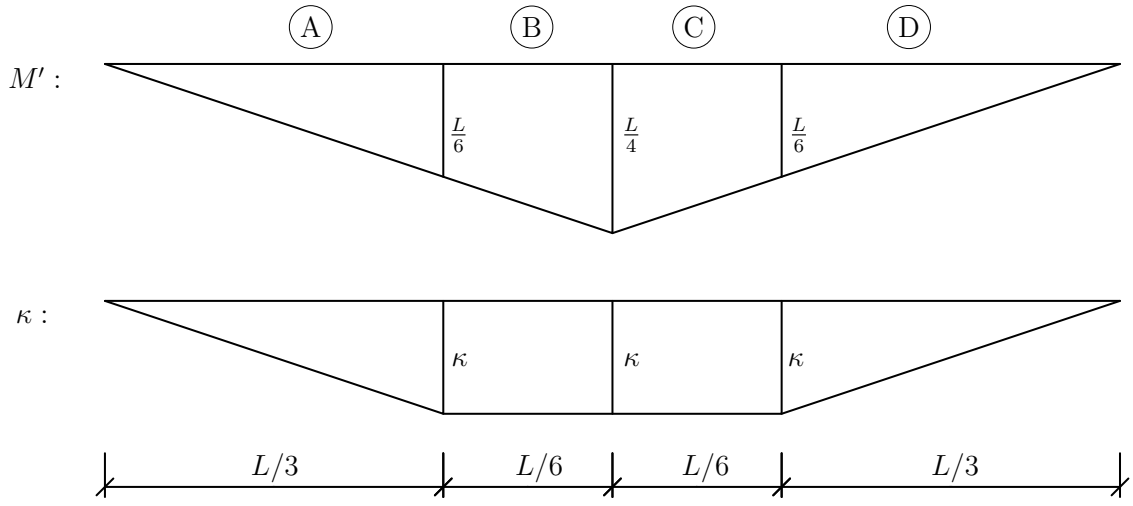

Figure 7: Moment diagram for a unit load applied at mid-span together with the curvature from two-point loading applied in the third-points of a simply-supported beam.

3.3 Experimental results

3.3.1 Reinforced SC-HFRC beams designed for flexural failure

Experimental load-deflection behaviour

The resulting load-deflection curves for the reinforced SC-HFRC beams designed for flexural failure are given in Figure 8. As expected, the beams of the 2.0 vol%-mix carries the highest load and are slightly stiffer. However, with respect to ductility, the beams of the 1.0 vol%-mix exhibits the best behaviour.

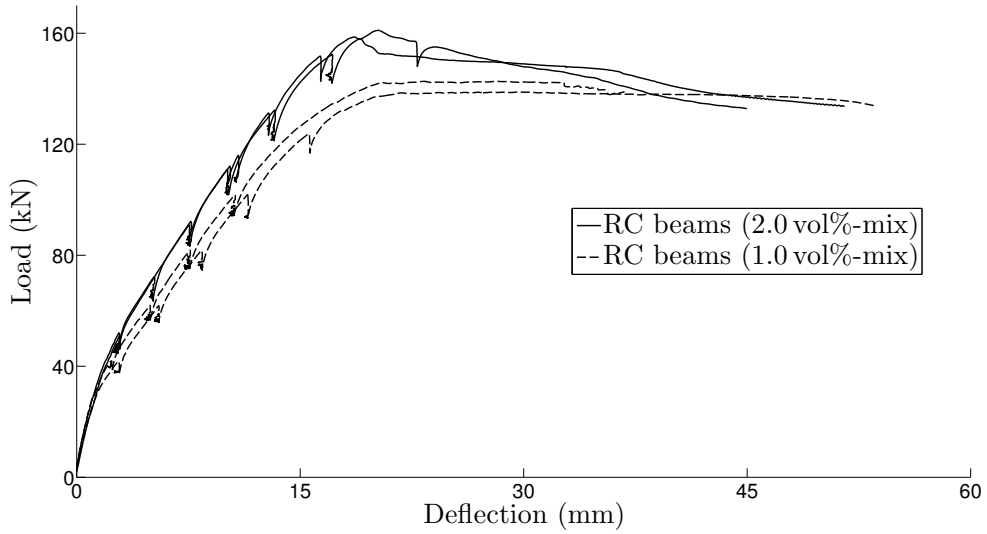

Figure 8: Experimental load-deflection curves for the reinforced SC-HFRC beams designed for flexural failure. It should be noted that the end of the curves do not represent collapse of the members, but simply that the tests was stopped.

Comparison with multi-layer model

Owing to the lack of a reference beam without fibres, the effect of fibres on the structural behaviour cannot be assessed directly. However, given that a precise estimate of the yield stress of the steel bars is available, the behaviour of an under-reinforced RC beam without fibres can be accurately predicted by the multi-layer model presented in section 2.3. According to tensile tests, the yield stress of the bars used in the tests was 566 MPa. The Youngs modulus was assumed to be 200 GPa and the post-yield behaviour was modelled as perfectly plastic. The compressive cylinder strength of the concrete was established by multiplying the average cube strength (determined from three 100 mm cubical specimens) by 0.8, while the residual tensile strength was an input variable (see Table 2). Other relevant material parameters for the concrete and the compressive stress-strain relation was derived from the compressive strength using Table 3 and clause 3.1.7 in EC2, respectively. The tensile stress-strain relation was modelled as linear elastic

followed by a constant 'yield' plateau equal to the residual tensile strength. The cross-section was divided into 1000 layers. In order to simulate the bending behaviour, the strain in the bottom layer was increased in steps of 0.1 ‰ until the tensile strain limit 3/h=0.01 for the FRC was reached. Within each step, the strain in the top layer was increased in increments of 0.01 ‰ until the sum of internal forces was less than $0.01\,kN$.

Figure 11 presents the results from the multi-layer analyses together with experimental moment-curvature relation for one 2.0 vol% beam and one 1.0 vol% beam. Both the experimental and the predicted curves are stopped at at the tensile strain limit $3/h$ for the fibre-reinforced cross-section (i.e. at a strain equal to 0.01 in the bottom layer). It can be seen that at this late stage in the bending behaviour, the contribution of the fibres to the load-carrying capacity is about 75% irrespective of the fibre content. This is partly due to the 2.0 vol% beams not being fully ductile and partly due to their lower than expected peak load-carrying capacity. Based on the measured residual tensile strength, the 2.0 vol% beams was expected to be 63.8/52.8=1.21 times stronger than the 1.0 vol% beams, but in reality they turned out to only be 80.5/71.3=1.13 times stronger. Hence, combined with the fact that the measured residual tensile strength only increased by a factor 3.3/1.9=1.74 by doubling the amount of fibres, it can be concluded that the use of the 2.0 vol% mix cannot be justified with respect to flexural behaviour in the ULS.

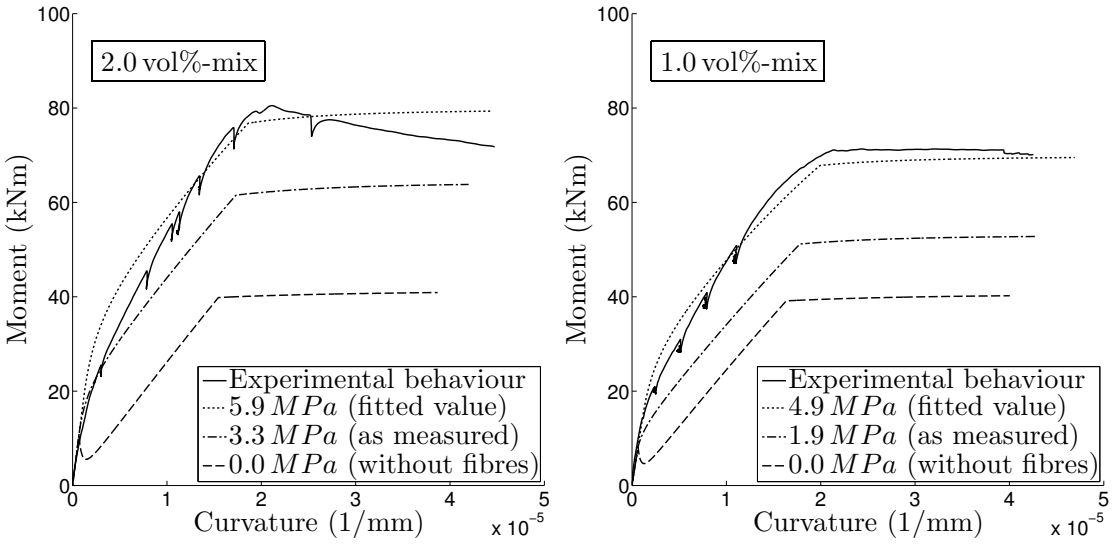

Figure 9: Experimental behaviour of one beam specimen of each mix compared to calculations according to the multi-layer procedure. The residual tensile strength in the calculations was either: fitted to match the experimental data; as measured in the EN 14651 tests; or zero in order to model the behaviour of a corresponding beam without fibres.

According to the analyses, the compressive strain at the tensile strain limit was 0.016, 0.026 or 0.034 for the 2.0 vol%-mix and 0.0021, 0.0029 or 0.0041 for the 1.0 vol%-mix, depending on the the value of the residual tensile strength. Hence, for the highest residual tensile strength, the predicted compressive strain for the 1.0 vol%-mix is higher than the compressive strain limit given in Table 3 in EC2. However, in this respect, it should be kept in mind that the compressive strain at failure is not really a material parameter but, simply, a safe lower-bound value for the maximum strain at the top of a RC beam in

bending. Moreover, it can also be seen that, in order to match the observed behaviour, the residual tensile strength had to be increased quite substantially compared to the corresponding value derived from the EN 14651 tests, especially for the 1.0 vol%-mix. The reason for this is, at least in part, a result of different fibre orientation in the material test specimens and the structural test specimens, e.g. due to different casting procedures, different aspect ratios of the cross-sections, and the presence of bar reinforcement in the structural test specimens. However, it might also be due to the incapability of the design assumptions to capture the observed behaviour.

Moment resistance according to design rule proposals

The moment resistance may alternatively be established from design rules. As a starting point, consider the hypothetical reference beam constructed with ordinary concrete with compressive strength equal to that of the 2.0 vol%-mix. For an under-reinforced RC beam without fibres, equilibrium of internal forces yields the following expression for the compressive depth

$$x = \frac{A_s f_y}{0.8 b f_c} = \frac{314 \cdot 566}{0.8 \cdot 200 \cdot 36.3} = \underline{30.6\, mm}$$

The moment resistance can then be obtained from equivalence between external and internal action

$$M_R = A_s f_y z = A_s f_y (d - 0.4x) = 314 \cdot 566 \cdot (245 - 0.4 \cdot 30.6) = \underline{41.4\, kNm}$$

As discussed in section 2.2, for a reinforced FRC beam, the only difference is that a tensile stress block is included in addition to the compressive stress block to account for the effect of fibres. The depth of the compressive zone is then given by

$$x = \frac{A_s f_y + b h f_{ft,res,2.5}}{0.8 b f_c + b f_{ft,res,2.5}} = \frac{314 \cdot 566 + 200 \cdot 300 \cdot 3.3}{0.8 \cdot 200 \cdot 36.3 + 200 \cdot 3.3} = \underline{58.1\, mm}$$

Further, equivalence between external and internal action yields

$$M_R = 314 \cdot 566(245 - 0.4 \cdot 58.1) + 200(300 - 58.1)3.3(0.1 \cdot 58.1 + 150) = \underline{64.3\, kNm}$$

The above equation corresponds to equation 5 in section 2.2 with $\lambda = 0.8$. In table 3 the calculated moment resistances for the various test specimens are compared to the corresponding experimental moment resistances at the peak load level.

Table 3: Experimental moment resistances at the peak load level, and the estimated counterparts according to the COIN report. All cross-sections are $b \times h = 200 \times 300\,mm$.

Batch nr.	Test age	f_c (MPa)	$f_{ft,res,2.5}$ (MPa)	d (mm)	A_s (mm^2)	f_y (MPa)	$M_{R,COIN}$ (kNm)	$M_{R,exp}$ (kNm)	$\frac{M_{R,exp}}{M_{R,COIN}}$
1	26	36.3	3.3	245	314	566	64.3	80.5	1.25
1	27	36.3	3.3	245	314	566	64.3	79.0	1.23
2	33	26.4	1.9	245	314	566	53.1	71.3	1.34
3	34	24.0	2.1	245	314	566	54.5	69.4	1.27

The calculated moment resistances are in accordance with the multi-layer predictions. This is not surprising, since the calculations and the analyses are based on similar assumptions. Hence, if the fitted residual strength in figure 11 is used in the design equations, the experimental values will be accurately predicted. However, the question arises on how to arrive at this value without the aid of structural data.

Crack calculations according to design rule proposals

Since the fibres mostly affect the post-cracking behaviour of the concrete, the cracking moment of a reinforced FRC cross-section can be calculated as for an ordinary RC cross-section without fibres. Consider an uncracked cross-section of the 2.0 vol%-mix. Moment of areas about the upper edge of the cross-section yields the height of the compressive zone

$$x = \frac{A_c \cdot 0.5h + \eta A_s d}{A_s + \eta A_s} = \frac{60000 \cdot 150 + 6.17 \cdot 314 \cdot 245}{60000 + 6.17 \cdot 314} = \underline{153\,mm}$$

The contribution of the concrete to the second moment of area is given by

$$I_{c1} = \frac{bh^3}{12} + bh\left(x - \frac{h}{2}\right)^2 = \frac{200 \cdot 300^3}{12} + 200 \cdot 300\left(153 - \frac{300}{2}\right)^2 = \underline{4.51 \cdot 10^8\,mm^4}$$

while the contribution of the longitudinal bar reinforcement is given by

$$I_{s1} = A_s(d - x)^2 = 314(245 - 153)^2 = \underline{2.66 \cdot 10^6\,mm^4}$$

The cracking moment can then by found through the expression

$$M_{cr} = \frac{I_{c1} + \eta I_{s1}}{h - x} \cdot f_{ct} = \frac{4.51 \cdot 10^8 + 6.17 \cdot 2.66 \cdot 10^6}{300 - 153} \cdot 3.3 = \underline{12.3\,kNm}$$

Table 7 lists the calculated cracking moments for the various test specimens. By comparing them to figure 11, it can be seen that the calculated values correspond quite well to the point where the moment-curvature relations starts to deviate from linearity. This supports the assumption that the cracking moment is not significantly influenced by the presence of fibres.

Table 4: Calculated cracking moment for the various test specimens. All cross-sections are $b \times h = 200 \times 300\,mm$. The direct tensile strength and the Youngs modulus for the concrete were established from the compressive strength by the expressions given in Table 3 in EC2.

Batch nr.	Test age	f_c (MPa)	f_{ct} (MPa)	E_c (MPa)	η (E_s/E_c)	d (mm)	A_s (mm^2)	M_{cr} (kNm)
1	26	36.3	3.3	32389	6.17	245	314	12.3
1	27	36.3	3.3	32389	6.17	245	314	12.3
2	33	26.4	2.7	29438	6.79	245	314	8.6
3	34	24.0	2.5	28608	6.99	245	314	8.0

An effect of the fibres, however, is to alter the bending stiffness of the cross-section after cracking. Hence, the bending stiffness may not be assumed to vary linearly with the loading as for ordinary RC beams. The compressive depth of the concrete and the stress in the flexural bars may therefore not be calculated as for an ordinary cracked RC cross-section. This hampers the calculations of crack widths. However, one solution is to extract these quantities from the multi-layer analyses. Using this approach, the strain difference between steel and concrete for a beam of the 2.0 vol%-mix may be calculated from the expression given in EC2 7.3.4(2)

$$\epsilon_{sm} - \epsilon_{cm} = \frac{243 - 0.6 \cdot \dfrac{3.3}{0.018}\,(1 + 6.17 \cdot 0.018)}{200000} = 0.62 \cdot 10^{-3} < 0.6 \cdot \frac{243}{200000} = \underline{0.73 \cdot 10^{-3}}$$

In the above, equation, the compressive depth of the concrete and the stress in the flexural bars were extracted from the multi-layer analysis at a load level equal to 60 % of the calculated peak load in table 3, since this corresponded to the load level at which the actual crack widths were measured. The factor k_t is set to 0.6 due to short-term loading. The maximum crack spacing can further be established from a formula similar to that given in EC2 7.3.4(3)

$$s_{r,max} = 3.4 \cdot 45 + 0.8 \cdot 0.5 \cdot 0.425 \left(1 - \frac{3.3}{3.3}\right) \frac{20}{0.023} = \underline{153\,mm}$$

where k_5 is an additional fibre contribution factor as deduced in section 2.2.3. From the above values, the resulting crack width is finally given by

$$w_k = 153 \cdot 0.73 \cdot 10^{-3} = \underline{0.11\,mm}$$

In Table 8 the calculated crack widths are presented together with their measured counterpart. The effective height, $h_{c,ef}$ in the calculation of the effective area of concrete in tension is governed by EC2 clause N.A.7.3.4, i.e. $h_{c,ef} = h - d + 1.5\phi$. It can be seen that the calculated values agree reasonably well with the experimental data, although the crack widths for the beams of the first batch was somewhat underestimated. This might be due to the fact that the mix from the first batch separated, which might have led to a lower direct tensile strength in the resulting test specimens. Further, it should be noted that the crack widths were measured using an optical comparator with an expected error in measurement equal to $\pm 0.005\,mm$. Hence, the procedure described above seems to be a feasible method for crack calculations in reinforced FRC. Especially when the average

Table 5: Calculated crack widths, at a load level equal to 60 % of the peak load, together with their experimental counterpart. All cross-sections are $b \times h = 200 \times 300\,mm$.

Batch nr.	f_c (MPa)	f_{ct} (MPa)	$f_{ft,res,2.5}$ (MPa)	x (mm)	σ_s (MPa)	$\epsilon_{sm} - \epsilon_{cm}$ (‰)	$s_{r,max}$ (mm)	$w_{k,COIN}$ (mm)	$w_{k,exp}$ (mm)
1	36.3	3.3	3.3	91.2	243	0.73	153	0.11	0.14
1	36.3	3.3	3.3	91.2	243	0.73	153	0.11	0.14
2	26.4	2.7	1.9	90.0	280	0.91	208	0.19	0.16
3	24.0	2.5	2.1	95.0	281	0.95	182	0.17	0.16

crack spacing is considered. In the COIN design approach, this value is calculated as for ordinary RC beams by dividing the maximum crack spacing by a factor 1.7. Hence, according to the calculations the mean value for the average crack spacing is equal to $90\,mm$ and $115\,mm$ for the beams of the 2.0 vol%-mix and the 1.0 vol%-mix, respectively. This is in good agreement with the measured values $89\,mm$ and $105\,mm$. One problem however is that the good predictions of the crack widths and spacings are obtained using the residual tensile strength as measured, while it had to be increased substantially in order to fit the experimental moment resistance.

3.3.2 Reinforced SC-HFRC slabs designed for flexural failure

Experimental load-deflection behaviour

The purpose of these tests was to examine if the residual tensile strength, as derived from the EN 14651 tests on small quadratic prisms, could be used to predict the behaviour of structural members with a totally different size and aspect ratio of the cross-section. The resulting load-deflection curves for the reinforced SC-HFRC slabs designed for flexural failure are given in figure 10.

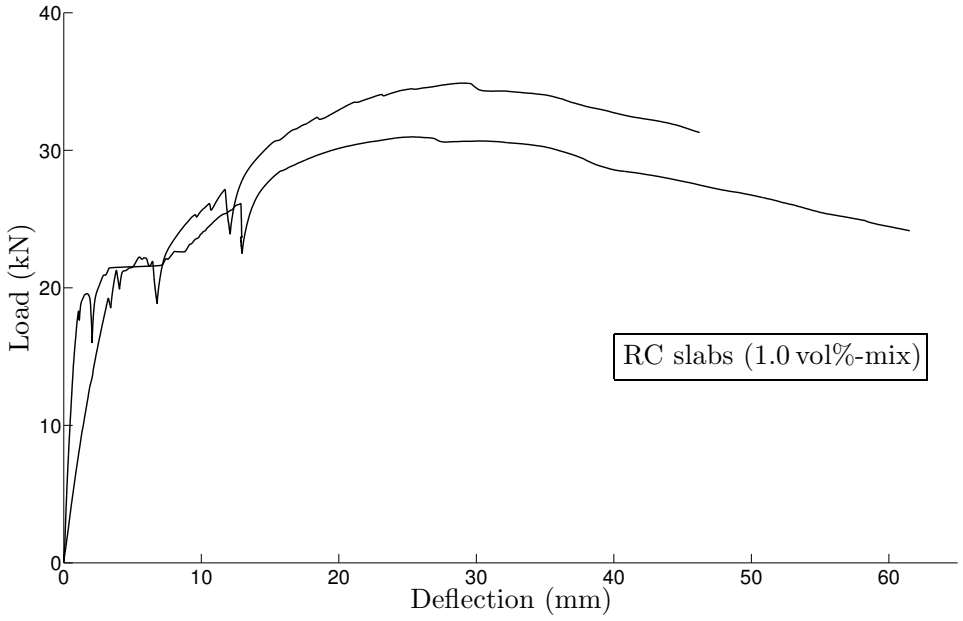

Figure 10: Experimental load-deflection curves for the reinforced SC-HFRC slabs designed for flexural failure. It should be noted that the end of the curves do not represent collapse of the members, but simply that the tests was stopped. The deflection is the sum of the upward deflection of the mid-section and the downward deflection at the loaded section.

Comparison with multi-layer model

For economical reasons, no reference RC slab without fibres was included in the test program. However, as for the structural beam specimens, given that a precise estimate of the yield stress of the flexural bars is available, the behaviour of an under-reinforced one-way RC slab without fibres can be accurately predicted by the multi-layer model presented in section 2.3. Unfortunately, no such measurements was available for the steel bars used in the slab specimens. Hence, the yield stress of the steel bars was assumed to be $500\,MPa$. This was deemed reasonable, since the load-carrying capacity anyway will be dominated by the contribution of the fibres owing to the low percentage of flexural steel bars. In all other respects, the multi-layer procedure was similar to that of the beam specimens.

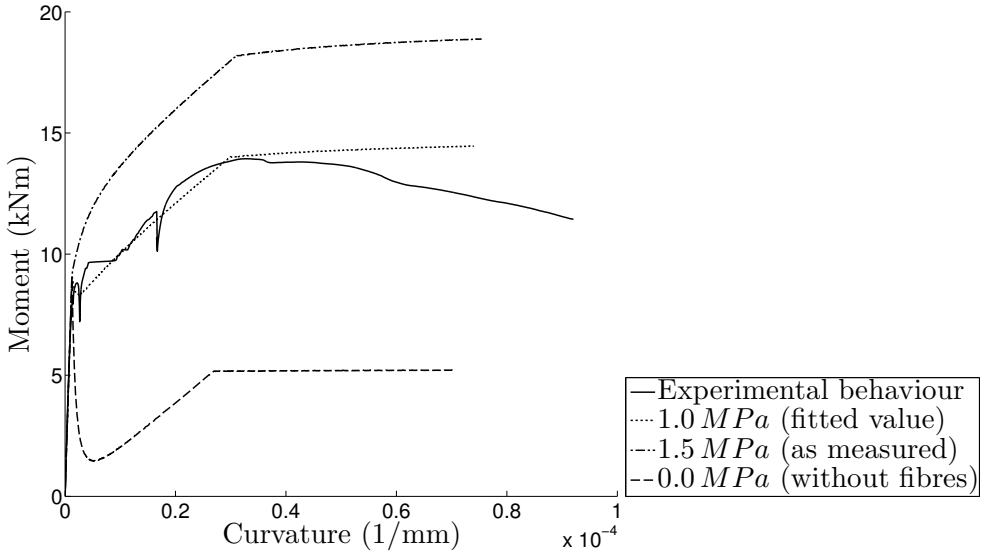

Figure 11: Experimental behaviour of one of the slab specimens compared to calculations according to the multi-layer procedure. The residual tensile strength in the calculations was either: fitted to match the experimental data; as measured in the EN 14651 tests; or zero in order to model the behaviour of a corresponding slab without fibres.

In Figure 11, the results from the multi-layer procedure are presented together with the experimental moment-curvature relation for one of the slab specimens. Both the experimental and the predicted curves are stopped at a strain equal to 0.01 in the bottom layer (i.e at the same strain as the flexural RC beam specimens). It can be seen that the load-carrying capacity at peak increase by a factor 13.9/5.2=2.67 due to the inclusion of fibres. However, this factor was predicted to be 18.9/5.2 = 3.63. This contradict the observations made for the flexural RC beams, where the effect of fibres were actually higher than predicted by the measured residual tensile strength.

Moment resistance according to design rule proposals

The moment resistance of the flexural one-way RC slabs may be established from design rules in the same manner as for the flexural RC beams. If the hypothetical reference slab is considered, the compressive depth of the concrete is given by

$$x = \frac{A_s f_y}{0.8 b f_c} = \frac{101 \cdot 500}{0.8 \cdot 900 \cdot 28.1} = \underline{2.5\, mm}$$

The moment resistance can further be obtained from equivalence between external and internal action

$$M_R = A_s f_y z = A_s f_y (d - 0.4x) = 101 \cdot 500 \cdot (106 - 0.4 \cdot 2.5) = \underline{5.3\, kNm}$$

For a corresponding reinforced FRC slab, the only difference is that a tensile stress block is included in addition to the compressive stress block to account for the effect of fibres. The depth of the compressive zone is then given by

$$x = \frac{A_s f_y + bh f_{ft,res,2.5}}{0.8 b f_c + b f_{ft,res,2.5}} = \frac{101 \cdot 500 + 900 \cdot 150 \cdot 1.5}{0.8 \cdot 900 \cdot 28.1 + 900 \cdot 1.5} = \underline{11.7\, mm}$$

Further, equivalence between external and internal action yields

$$M_R = 101 \cdot 500(106 - 0.4 \cdot 11.7) + 900(150 - 11.7)1.5(0.1 \cdot 11.7 + 75) = \underline{19.3\, kNm}$$

In table 6 the calculated moment resistances for the two slab specimens are compared to the corresponding experimental moment resistances at the peak load level.

Table 6: Experimental moment resistances at the peak load level and the estimated counterparts according to the COIN report. All cross-sections are $b \times h = 900 \times 150\, mm$.

Batch nr.	Test age	f_c (MPa)	$f_{ft,res,2.5}$ (MPa)	d (mm)	A_s (mm^2)	f_y (MPa)	$M_{R,COIN}$ (kNm)	$M_{R,exp}$ (kNm)	$\frac{M_{R,exp}}{M_{R,COIN}}$
2	50	29.2	1.9	106	101	500	19.3	14.3	0.74
4	34	28.1	1.5	106	101	500	19.3	11.4	0.59

As already mentioned, contrary to the beam specimens, the measured value of the residual tensile strength overestimates the moment resistance for the slab specimens quite substantially. Hence, by comparing the results in table 3 and 6, it might be hypothesized that a cross-section with a high b/h-ratio is likely to have an unfavourable orientation of fibres in the structure. This will be discussed further in the subsequent section, where the actual orientation of fibres in the structural members are sought determined experimentally.

Crack calculations according to design rule proposals

Consider an uncracked section of the slab specimen from batch 4. Moment of areas about the upper edge of the cross-section yields the height of the compressive zone

$$x = \frac{A_c \cdot 0.5h + \eta A_s d}{A_s + \eta A_s} = \frac{135000 \cdot 75 + 6.67 \cdot 101 \cdot 106}{135000 + 6.67 \cdot 101} = \underline{75.1\, mm}$$

The contribution of the concrete to the second moment of area is given by

$$I_{c1} = \frac{bh^3}{12} + bh\left(x - \frac{h}{2}\right)^2 = \frac{900 \cdot 150^3}{12} + 900 \cdot 150\left(75.1 - \frac{150}{2}\right)^2 = \underline{2.53 \cdot 10^8\, mm^4}$$

while the contribution of the longitudinal bar reinforcement is given by

$$I_{s1} = A_s(d-x)^2 = 101(106-75.1)^2 = \underline{96.4 \cdot 10^3\, mm^4}$$

The cracking moment can then by found through the expression

$$M_{cr} = \frac{I_{c1} + \eta I_{s1}}{h-x} \cdot f_{ct} = \frac{2.53 \cdot 10^8 + 6.67 \cdot 96.4 \cdot 10^3}{150 - 75.1} \cdot 2.8 = \underline{9.5\, kNm}$$

Table 7 lists the calculated cracking moments for the various test specimens. By comparing them to figure 11, it can be seen that the calculated values correspond quite well to the point where the moment-curvature relations starts to deviate from linearity. Hence, as for the beam specimens, the cracking moment do not seem to be significantly influenced by the presence of fibres.

Table 7: Calculated cracking moment for the various flexural slab specimens. All cross-sections are $b \times h = 900 \times 150\, mm$.

Batch nr.	Test age	f_c (MPa)	f_{ct} (MPa)	E_c (MPa)	η (E_s/E_c)	d (mm)	A_s (mm^2)	M_{cr} (kNm)
2	50	29.2	2.8	30342	6.59	106	101	9.5
4	34	28.1	2.8	29994	6.67	106	101	9.5

Moreover, as for the beam specimens, the multi-layer method can be used to determine the compressive depth of the concrete and the stress in the flexural bars. The strain difference, needed for the calculation of crack widths, may then be obtained through the the expression given in EC2 7.3.4(2)

$$\epsilon_{sm} - \epsilon_{cm} = 0.6 \cdot \frac{329}{200000} = \underline{0.99 \cdot 10^{-3}}$$

In the above, equation, the stress in the flexural bars were extracted from the multi-layer analysis at a load level equal to 84 % of the calculated peak load in table 6, since this corresponded to the load level at which the actual crack widths were measured. Since the distance between the reinforcement bars is larger than $5(c + \phi/2)$, the maximum crack spacing may further be established from the upper bound value given in EC2 7.3.4(3)

$$s_{r,max} = 1.3 \cdot (h-x) = 1.3 \cdot (150 - 28.6) = \underline{158\, mm}$$

Finally, from the above values, the resulting crack width is given by

$$w_k = 158 \cdot 0.99 \cdot 10^{-3} = \underline{0.16\, mm}$$

Table 8: Calculated crack widths, at a load level equal to 78 % and 84 of the peak load for the two specimens respectively, together with their experimental counterpart. All cross-sections are $b \times h = 900 \times 150\,mm$.

Batch nr.	f_c (MPa)	f_{ct} (MPa)	$f_{ft,res,2.5}$ (MPa)	x (mm)	σ_s (MPa)	$\epsilon_{sm} - \epsilon_{cm}$ (‰)	$s_{r,max}$ (mm)	$w_{k,COIN}$ (mm)	$w_{k,exp}$ (mm)
2	29.2	2.8	1.9	46.9	76.8	0.23	134	0.03	0.16
4	28.1	2.8	1.5	28.6	329	0.99	158	0.16	0.14

In Table 8 the calculated crack widths are presented together with their measured counterpart. The effective height, $h_{c,ef}$ in the calculation of the effective area of concrete in tension is governed by the lower limit, $h_{c,ef} = h - d + 1.5\phi$, in EC2clause N.A.7.3.4, whereas the maximum crack spacing is governed by the upper limit $s_{r,max} = 1.3(h - x)$ in EC2 clause 7.3.4(3). It is interesting to note that the while the crack width is well predicted for one specimen, the prediction for the other is totally off. This suggests that the calculation procedure is not suited for FRC cross-sections with a very low percentage of bar reinforcement, since the calculation of the stress in the flexural bars is all too sensitive to the value of the residual tensile strength. Moreover, the average crack spacing was badly predicted for both specimens: the calculated values were $134/1.7 = 79\,mm$ and $158/1.7 = 93\,mm$ respectively, while the measured counterparts were $137\,mm$ and $127\,mm$.

3.3.3 Reinforced SC-HFRC beams designed for shear failure

Experimental load-deflection behaviour

The resulting load-deflection curves for the reinforced SC-HFRC beams designed for shear failure are given in Figure 12.

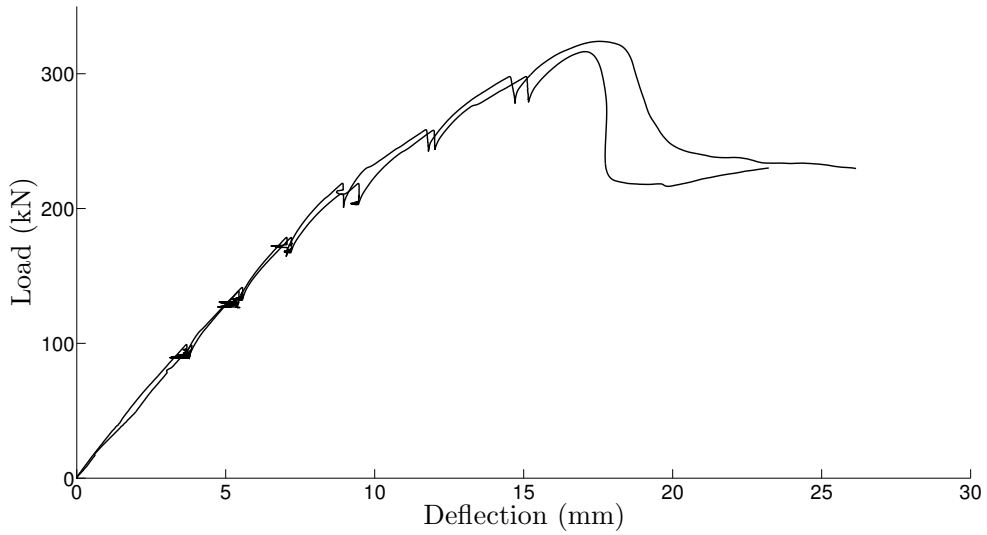

Figure 12: Experimental load-deflection curves for the reinforced SC-HFRC beams designed for shear failure.

Shear resistance according to design rule proposals

The shear resistance can be calculated according to the design rules given in section 2.2.2. For an ordinary RC beam without stirrups the shear resistance is given by

$$V_{Rd,ct} = [0.15 \cdot 1.93 \cdot (100 \cdot 0.02 \cdot 25.4)^{1/3}] \cdot 200 \cdot 228 = \underline{48.9\,kN}$$

The effect of fibres is accounted for by the expression

$$V_{Rd,cf} = 0.6 \cdot 1.5 \cdot 200 \cdot 300 = \underline{54.0\,kN}$$

By taking these two values together, the shear resistance for the reinforced SC-HFRC beam is obtained. In table 9 the calculated shear resistances for the two test specimens are compared to the shear resistance obtained in the experiments.

Table 9: Experimental shear resistance for the two test specimens and their estimated counterpart according to the COIN design approach. All cross-sections are $b \times h = 200 \times 300\,mm$.

Batch nr.	Test age	f_c (MPa)	$f_{ft,res,2.5}$ (MPa)	d (mm)	A_s (mm^2)	$V_{R,t}$ (kN)	$V_{R,f}$ (kN)	$V_{R,COIN}$ (kN)	$V_{R,exp}$ (kN)
4	19	25.4	1.5	228	1609	48.9	54.0	103	160
5	20	21.4	1.6	228	1609	46.2	57.6	104	164

It can be seen that the experimental resistance is about 60 % greater than the calculated values. This is to be expected when a simple semi-empirical equation are to provide a safe lower-bound value to a wide range of applications. The most important thing is therefore that the calculated values are on the safe side.

3.3.4 Estimated residual tensile strength from fibre counting

The actual fibre content in both the En 14651 prisms and the structural test specimens, may be obtained by crushing a given cross-sectional piece to extract the fibres and then simply weigh the extracted fibres. Then, if the density of the fibres is known, the fibre content by volume may easily be calculated for the given piece using the relation $\rho = m/V$. This has not been done for the specimens in the test program. Hence, the fibre content in the EN 14651 prisms, ν_f, and the actual fibre content in the structural members, $\nu_{f,struct}$, are assumed to be equal to the nominal fibre content, $\nu_{f,nom}$, according to mix design.

The corresponding fibre orientation factors, on the other hand, were determined experimentally by counting the fibres crossing one of the sawn surfaces of the cross-sectional piece taken out of the member. The procedure was as follows; cover the exposed surface with a plastic film; mark the cut fibre cross-sections with a marker; attach a white paper sheet to the back of the plastic film for increased contrast and scan it. The number of dots, i.e. the number of fibres crossing the cross-section, may then be found using an image processing tool or, as a more tedious alternative, by manual counting.

The fibre orientation factor is simply the counted number divided by the the number of fibres according to the fibre content. Hence, if all the fibres in a cross-section bridge across the exposed surface, the fibre orientation factor should be equal to 1. Contrary, if no fibres bridge across this surface, the fibre orientation factor will be 0. The in-between case, $\alpha = 0.5$, means that the fibres have no preferred direction in the material, i.e. the FRC in the cross-sectional piece taken out of the member is isotropic.

The fibre content of a cross-section is given by the relation

$$\nu_f = \frac{n \cdot A_f}{A_c} \tag{18}$$

By rearranging this equation, the cross-sectional number of fibres according to the fibre content may be obtained through the relation

$$n = \nu_f \cdot \frac{A_c}{A_f} \tag{19}$$

where A_f is the cross-sectional area of a single fibre and A_c is the cross-sectional area of the concrete. The cross-sections of a Dramix 65/60 fibre and a Barchip Shogun 48 fibre are $0.64\,mm^2$ and $0.76\,mm^2$, respectively. Hence, if a 50/50 distribution is assumed (as in the mix design), the maximum number of fibres for a given cross-section can be determined from the above equation. By relating the counted number of fibres in the section to this number, the fibre orientation factor is obtained. The reason for determining the fibre orientation factors for the material and structural specimens is to adjust the residual tensile strength, as measured in the EN 14651 tests, such that it corresponds to the actual condition in the structure. By combining equation 3 and 4 in section 2.1, the following relation is obtained

$$f_{ftk,res,2.5,struct} = f_{ftk,res,2.5} \cdot \overbrace{\frac{\nu_{f,struct}(4\alpha_{struct} - 1)}{\nu_f(4\alpha - 1)}}^{\xi} \tag{20}$$

where the latter term is a factor which account for the different orientation of fibres in the structure and in the EN 14651 prisms.

In table 10 the results from the fibre counting are presented. The specimens from batch 1 are not included, since the fibres were not counted for these members. For the other flexural members, i.e. the beams from batch 2 and 3 and the slabs, the fibres were counted at mid-span, since this was considered to be the critical section. The critical section for the shear beams, on the other hand, was deemed to be 500 mm from the support in the shear-span that failed. However, since this section was highly cracked, the cross-sectional piece was taken out on from the corresponding section in the opposite end of the beam. For the EN 14651 prisms the fibres were counted in a section next to the notch.

Table 10: Correction factor for the measured residual tensile strength according to counting of fibres in the critical sections of the structural specimens and the EN 14651 prisms.

Batch	Member	Structural specimens			EN 14651 prisms			$f_{ft,res,2.5}$	$f_{ft,res,2.5,struct}$	
nr.	type	n_{count}	n	α_{struct}	n_{count}	n	α	(MPa)	ξ	(MPa)
2	Beam	668	863	0.77	292	324	0.90	1.9	0.80	1.5
3	Beam	712	863	0.83	273	324	0.84	2.1	0.98	2.1
4	Beam	587	863	0.68	230	324	0.71	1.5	0.93	1.4
5	Beam	604	863	0.70	242	324	0.75	1.6	0.90	1.4
2	Slab	1442	1943	0.74	292	324	0.90	1.9	0.75	1.4
4	Slab	1150	1943	0.59	230	324	0.71	1.5	0.73	1.1

It can be seen that the residual tensile strength, as measured in the EN 14651 tests, is reduced for all specimens, but to the largest degree for the slab specimens.

Prior to the corrections, the strengths of the structural beam and slab specimens were underestimated and overestimated, respectively. This means that while the predicted strength values of the beam specimens become slightly more conservative after the correction, the predicted strengths of the the slab specimens are approaching their experimental values.

3.4 Conclusions

The motivation behind the test program presented in this section was to investigate if the residual tensile strength, as derived from the EN 14651 tests, could be used to predict the effect of fibres in structural members made of highly ductile SC-HFRC. An important finding was that whereas the load-carrying capacity of the flexural beam specimens was underestimated, the load-carrying capacity of the flexural slab specimens was overestimated. This was not surprising, since a cross-section with a high b/h-ratio is expected to have a more isotropic fibre distribution due to reduced wall effect.

When the residual tensile strength was corrected for fibre orientation, the predicted moment resistance for the slab specimens approached the experimental value, whereas the predictions for the beam specimens became slightly more conservative. The predicted resistance for the shear beams was about 64 % of the experimental value before correction and a little less after.

Another interesting finding was that, the moment resistance at the tensile strain limit 3/h for the flexural beam containing 1.0 vol% fibres was equal to the flexural beam containing 2.0 vol% fibres. Hence, the high amount of fibres cannot be justified, at least not when it comes to the flexural behaviour. However, it should be noted that the 2.0 vol%-mix segregated during mixing due to excessive use of superplasticizer, which might have led to an inferior structural behaviour.

Moreover, it was argued that the multi-layer beam model could be used as a tool to determine the stress in the flexural bars and the compressive depth needed in the crack-width control. By using this procedure, and by adding an extra factor to account for the effect of fibres in the crack spacing formula, it was shown that the crack widths for the flexural beam specimens could be satisfactorily predicted. However, for the flexural slab specimens, the amount of steel bars was so low that the stress in these became highly dependent on the actual residual tensile strength of the concrete, which led to more or less arbitrary results.

It should be noted that simple design rules are not expected to be able to fit all experimental data. The most important thing is therefore that they are safe for a wide range of applications. It is therefore not alarming that some of the estimated values are quite conservative. Hence, the COIN design approach seems to be provide an adequate set of rules, at least for the investigated members, with the exception of the lightly reinforced flexural slab specimens for which the results were non-conservative.

4 Reinforced FRC beams with dapped ends

4.1 Introduction

Precast dapped-end RC beams have many useful applications: e.g. as drop-in beams between corbels, as part of beam-to-beam connections or in suspended spans between cantilevers [10]. Dapped ends enables the construction height of a precast concrete floor or roof structure to be reduced, by recessing the supporting corbel or ledge into the depth of the supported beam and facilitates the erection of a precast concrete structure due to the greater lateral stability of a dapped member [11]. However, as illustrated in figure 13, the nib at the end of the beam results in a severe stress concentration at the re-entrant corner. This can initiate diagonal tension cracking at a lower shear than would otherwise be expected. Hence, if suitable reinforcement is not provided close to the re-entrant corner, failure can occur with little or no warning [12].

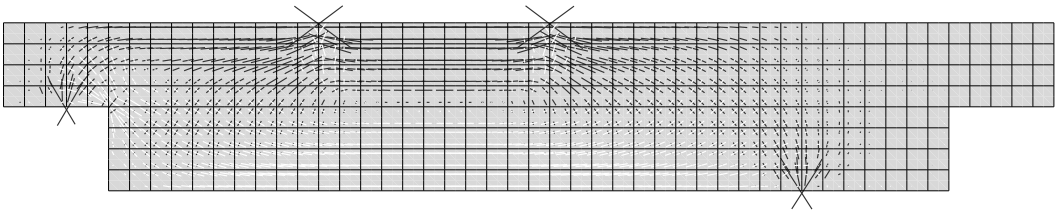

Figure 13: Principal stresses of a symmetric dapped beam under asymmetrical four-point loading according to elastic analysis using under-integrated quadratic plane-stress elements. The large stress concentrations at the point loads is not representative, since the loading in reality is not that sharp.

Since placing of this reinforcement is laborious and often complicated, it would be highly advantageous if some of the traditional bar reinforcement could be substituted by fibres. Although a lot of research exists on the structural performance of FRC, only a few tests have been conducted to study the performance of dapped-end RC beams with fibres [13],[14],[15],[16]. An experimental program was therefore undertaken to investigate the effect of fibres on the response of dapped-end RC beams with reduced amount of traditional bar reinforcement. Moreover, FRC for structural applications has yet to gain wide acceptance due to lack of proper design rules in codes and standards. Hence, a strut-and-tie model (STM), which accounts for the shear-resistance provided by the fibres, is proposed and further validated against the experimental results.

4.2 Experimental program

4.2.1 Brief overview

A series of eight dapped ends were tested to investigate if fibres could be used to simplify the detailing of precast dapped-end beams. Three types of concrete were included in the

test program: an ordinary concrete for reference; a SC-SFRC with 1.0 vol% steel fibres; and a SC-HFRC with 0.75 vol% steel fibers and 0.75 vol% synthetic fibres. The reinforcement layout was either: (1) according to general practice in the Norwegian precast industry; (2) with reduced hanger and anchorage reinforcement and no inclined reinforcement or horizontal stirrups; (3) as previous but without hanger reinforcement; (4) as the second layout but mid-centered to optimise for fibre flow and with a slightly larger diameter of the hanger reinforcement. The fibre-reinforced specimens of layout 2 and 4 performed nearly as well as their conventionally reinforced counterpart, proving the feasibility of the concept. However, there was almost no difference in behaviour between the two fibre concretes, indicating that steel fibres are to be preferred.

4.2.2 Design according to Norwegian practice

In Norway, guidelines for the design and construction of precast concrete structures is published by the trade association for the Norwegian precast concrete manufacturers. Section 8.2 of part C of these publications gives design guidelines for dapped-end beams based on strut-and-tie modelling [17]. In Figure 14, the chosen dimensions for the dapped ends in the test program are depicted.

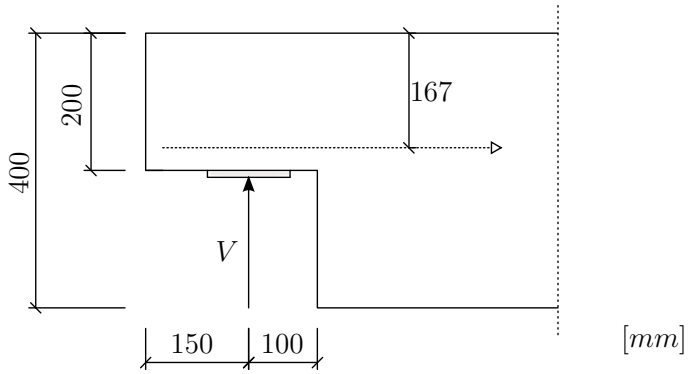

Figure 14: Dimensions for the dapped-ends in the test program. The nib and the full-depth beam has a rectangular cross-section $b \times h = 250 \times 200\,mm$ and $B \times H = 250 \times 400\,mm$, respectively. A $120 \times 200mm$ plastic plate is used as insert between the dapped end and the base.

The distance from the centre of support to the interface between the nib and the full depth beam is $a_0 = 100\,mm$. Moreover, if ø16 bars with $25\,mm$ cover are used as main nib reinforcement, the effective depth of the nib becomes $d = 167\,mm$. For the design rules in section 8.2.1 to be applied, a_0/d must not be greater than unity and the horizontal reaction, H, at the support must not be greater than the vertical reaction V. This is fulfilled for the dapped ends in the test program, since they only are subjected to a vertical reaction and $a_0/d = 0.60$[3]. Moreover, it is recommended that the depth of the

[3]In a real design situation, however, the horizontal force should be taken as $0.15V$ (or $0.20V_g$ whichever greatest) owing to the possibility of frictional forces and, moreover, a_0 should be increased by $20\,mm$ to account for unintended eccentricity in loading.

nib is not less than half the full-depth of the beam and that the length of the nib is less than $0.7h$. For the chosen dimensions, the former criteria is just satisfied, whereas the length of the nib is almost twice the recommended value.

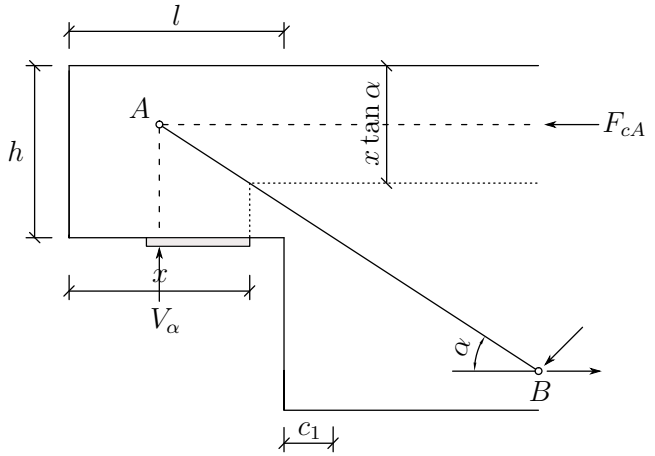

Figure 15: Strut-and-tie model which account for the part of the vertical reaction carried by the inclined hangers. Compressive struts are dashed, whereas tensile ties are indicated by solid lines.

Reinforcement schemes using inclined hanger reinforcement provide better crack control than the ones with only vertical hangers [12]. Hence, in Norway, it is usual to let the vertical reaction be carried by a combination of vertical and inclined hangers. In this case, the combination of two strut-and-tie models for the dapped beam is better than an individual model [18]. Figure 15 depicts the model which account for the part of the vertical reaction, V_α, carried by the inclined hangers AB. The recommended angle of the inclined hangers is given by

$$\tan\alpha = \frac{h}{l+c1} = \frac{200}{250+(33+4+20)} \rightarrow \alpha = \underline{33.1^\circ} \tag{21}$$

where h and l is the depth and length of the nib and c_1 is the distance from the beam-nib interface and the centroid of the vertical hangers. In the above equation, it has been assumed two ø8c40 stirrups with 33 mm cover as vertical hangers. Further, if two inclined ø10 hangers is assumed, the shear resisted is simply given by the vertical component of their yield force

$$V_\alpha = F_{AB}\cdot\sin\alpha = A_s\cdot f_y\cdot\sin\alpha = 2\pi 5^2\cdot 500\cdot\sin 33.1 = \underline{42.9\,kN} \tag{22}$$

Hence, although it is the reinforcement which actually resists V_α, the concrete must still be able to provide a sufficient thrust to keep the truss from collapsing. The stress in the horizontal compressive strut due to the shear resisted by the inclined hangers is given by

$$\sigma_{c\alpha} = \frac{F_{cA}}{A_c} = \frac{\frac{V_\alpha}{\tan\alpha}}{b\cdot x\tan\alpha} = \frac{\frac{42.9\cdot 10^3}{\tan 33.1}}{250\cdot 210\cdot\tan 33.1} = \underline{1.92\,MPa} \tag{23}$$

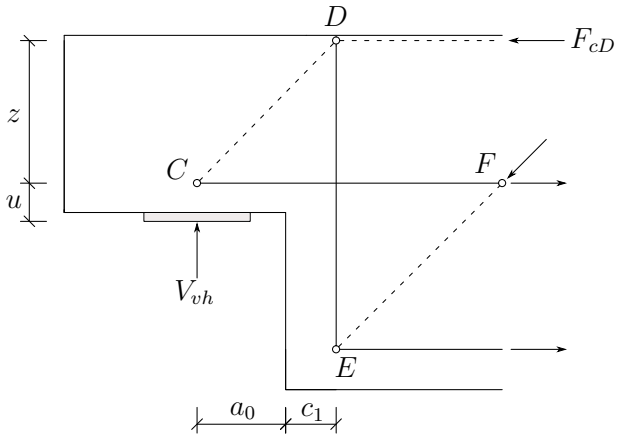

Figure 16: Strut-and-tie model which account for the part of the vertical reaction carried by the vertical hangers. Compressive struts are dashed, whereas tensile ties are indicated by solid lines. The horizontal external tensile restraint at node F is provided by the development length extension of tie CF [19].

which is well below the compressive strength of the concrete.

Figure 16 depicts the model which account for the part of the vertical reaction, V_{vh}, carried by the vertical hangers DE. In this case, it is the vertical component of the inclined compression in the nib which resists the shear. However, in order for it to do so, it must be balanced by the tension force in the vertical hangers. Hence, the shear force that can be balanced by the two ø8 stirrups is given by

$$V_{vh} = F_{DE} = 2 \cdot 2\pi 4^2 \cdot 500 = \underline{101\,kN} \tag{24}$$

which is above $2/3V$ as recommended [20]. Moreover, the main nib reinforcement must be designed so as to balance the outward thrust of the inclined compression leg (and the horizontal reaction, H, should it exist). If the horizontal strut is taken to be fully utilised at yield of the vertical hangers, the internal level arm may be approximated as

$$z \approx d - \frac{V_{vh} \cdot \overbrace{(a_0 + u\frac{H}{V} + c_1)}^{a'}}{1.6 \cdot b \cdot d \cdot (f_c - \sigma_{c\alpha})} = 167 - \frac{101 \cdot 10^3 \cdot (100 + 57)}{1.6 \cdot 250 \cdot 167 \cdot (0.85 \cdot 43.2 - 1.92)} = \underline{160\,mm} \tag{25}$$

where the compressive depth has been determined from horizontal equilibrium at D with compressive strength $0.85f_c$ as defined in EC2 clause 6.5.4(4) and by initially assuming $z = 0.8d$. The force in the main nib reinforcement corresponding to yield of the vertical hangers is then given by

$$F_s = F_{CF} + H = \frac{V_{vh} \cdot a'}{z} + H = \frac{101 \cdot 10^3 \cdot (100 + 57)}{160} + 0 = \underline{99.1\,kN} \tag{26}$$

However, in the test specimens, two ø16 bars were used as main nib reinforcement, which is equivalent to $F_s = 2\pi 8^2 \cdot 500 = 201\,kN$. This means that the main nib reinforcement

is about twice the necessary amount which makes it very unlikely to yield before failure of the dapped end in the tests. Another unwanted failure mode in the tests is failure of the inclined compressive leg. This can be checked for by using the formula given in EC2 clause 6.2.2(6) as follows

$$V_{max} = 0.5 \cdot b_w \cdot d \cdot \nu \cdot f_c = 0.5 \cdot 250 \cdot 167 \cdot 0.6 \left(1 - \frac{43.2}{250}\right) \cdot 43.2 = \underline{448\,kN < V} \quad (27)$$

where the softening effect due to transverse tensile stress is accounted for by the factor ν. Further, to avoid a premature diagonal tension or 'diagonal splitting' failure of the nib, horizontal stirrups or ties should be placed in an amount equal to

$$A_h = 0.5 \cdot A_s = 0.5 \cdot \frac{F_{CF}}{f_y} = 0.5 \cdot \frac{99.1 \cdot 10^3}{500} = \underline{99.1\,mm^2} \quad (28)$$

In the reference beam, two u-shaped ø8c50 closed ties were used, which is twice the recommended amount. Moreover, one u-shaped ø8 tie were used to secure proper end anchorage of the vertical hangers, which corresponds to half the suggested value

$$A_{se} = A_{vh} = \frac{V_{vh}}{f_y} = \frac{101 \cdot 10^3}{500} = \underline{202\,mm^2} \quad (29)$$

Figure 19 depicts the resulting reinforcement layout. The dapped-end reinforcement is as described in the calculations, whereas three ø25 bars with 33 mm cover is used as beam flexural reinforcement, two ø8 bars with 33 mm cover is used as beam compressive reinforcement, and six ø8c250 stirrups is used as beam shear reinforcement. In addition, one ø8 stirrup is placed at the end of the main nib reinforcement for mounting purposes. The main-nib reinforcement is welded to a crossbar at the left end in order to prevent if from slipping in the concrete.

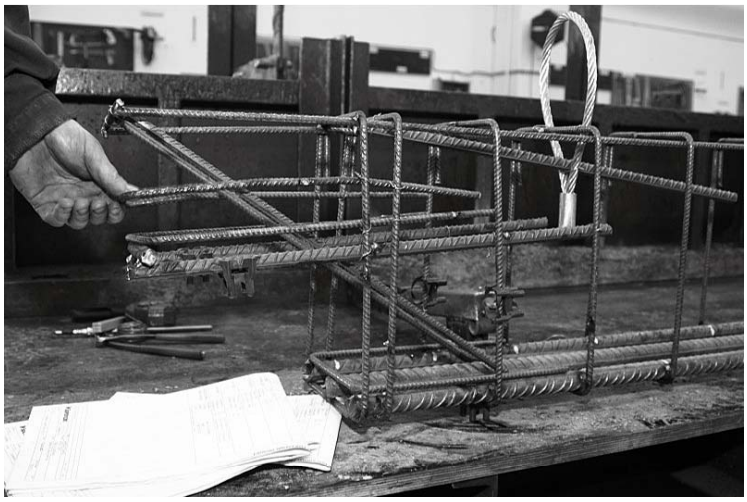

Figure 17: Reinforcement layout according to common practice in the Norwegian precast industry. The steel wire is a lifting hoop used when moving the specimens.

4.2.3 Details of test specimens

The dapped ends were tested under static loading as shown in figure 18. The specimens were 250 mm wide, 400 mm deep with a total length of 2500 mm. The loading arrangement and reinforcement layout was chosen such that failure occurred in the region of the left dapped end of all specimens. Moreover, since the damage was mostly confined to this region, the beam could be reverted after testing and the test repeated for the other end. The various reinforcement layouts investigated in the test program are depicted in figure

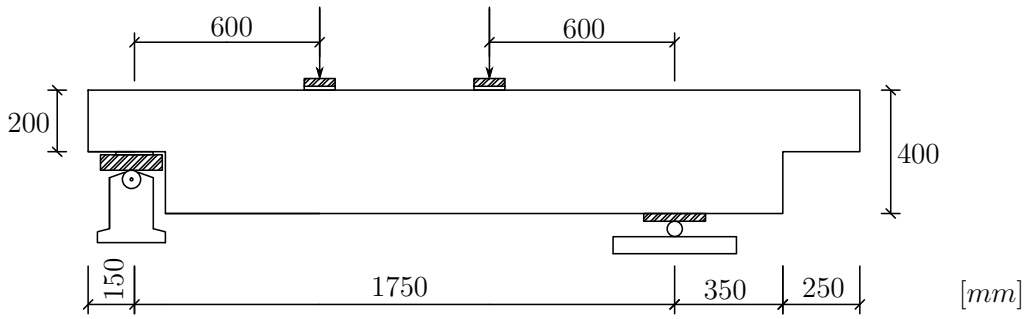

Figure 18: Test set-up for the dapped-end RC beams. The left support is pinned while the right support is free to translate horizontally.

19. The main test variables were the amount and placing of the hanger reinforcement and the type of concrete. Although the conventionally reinforced beam is provided with beam shear reinforcement, this is not considered to influence the structural behaviour to any notable degree, since the dapped-end anyway will be critical.

4.2.4 Materials

Details of the mix design for the SC-SFRC and the SC-HFRC are given in Table 11. It can be be seen that the effective water-cement ratio is about 0.48 for both mixes.

Table 11: Composition of the different concretes utilised in the test program. All components are specified by its dry content except for water.

Components in kg/m^3	SC-SFRC (1.0 vol%)	SC-HFRC (1.5 vol%)
Norcem standard cement (FA)	470	465
Elkem microsilica 940U	18.8	18.6
Effective water	224	227
Absorbed water	14.8	14.7
Kveldstad aggregate $(0-8\,mm)$	1322	1308
Limestone aggregate $(7-14\,mm)$	323	320
Sica Viscocrete	1.1	1.1
Dramix 65/60 steel fibres	78.0	58.5
Barchip 48 synthetic fibres	-	6.9
Total weight	2452	2420

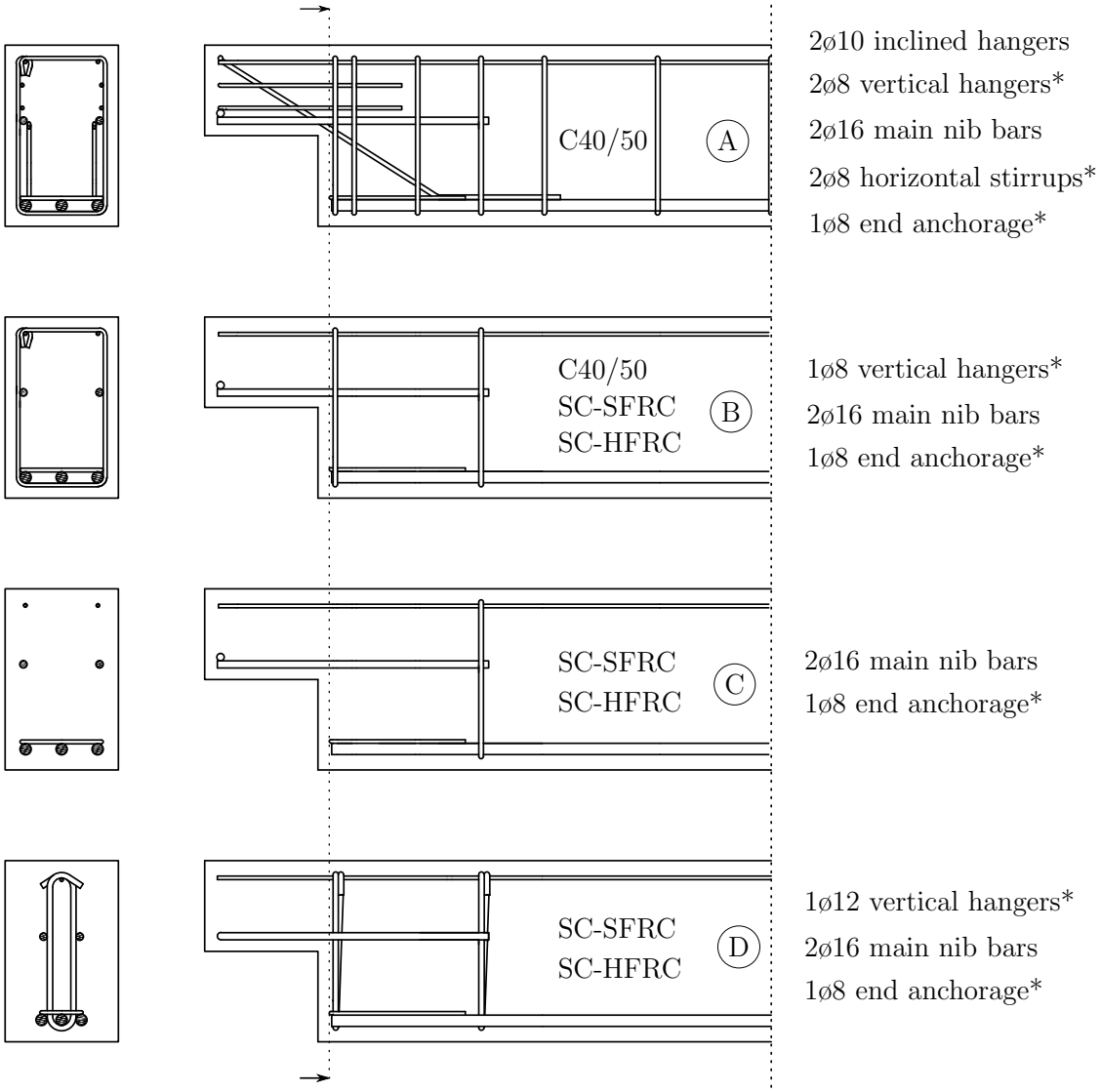

Figure 19: Variables investigated investigated in the test program. The dapped-end reinforcement and the type of concrete varied as described in the text, whereas the beam beam reinforcement (except for the beam shear reinforcement) remained constant. Reinforcement marked with a star indicates that it is stirrups (i.e. double-legged reinforcement).

Dramix 65/60 is a cold drawn steel wire fibre with hooked ends (length $l = 60\,mm$, aspect ratio $l/d = 67$, tensile strength $\sigma_t = 1000\,MPa$), whereas Barchip shogun is a synthetic polymeric fibre with embossed surface texture (length $l = 48\,mm$, tensile strength $\sigma_t = 550\,MPa$, Youngs modulus $E = 10\,GPa$). Sica Viscocrete is a high range water reducing superplasticizer. It was added in an amount corresponding to 1.6 % of the cement weight, i.e. about $7.5\,kg/m^3$. Its dry content is about 15 %. Hence, in table 11 the amount is given as $0.016 \cdot 470 \cdot 0.15 = 1.1\,kg/m^3$. The remaining water is included in the effective water.

4.2.5 Testing of specimens

All specimens were tested under four-point loading, as shown in figure 18, using a 1000 kN capacity hydraulic jack. The loading was displacement controlled at a rate of 0.008 mm/s. To measure the load applied to the spreader beam, the load cell of the testing machine was used. A linear voltage differential transducer (LVDT) was used to measure the vertical deflection midway between the supports, allowing the overall load-deflection behaviour of the specimens to be determined. Moreover, electrical resistance strain gauges were used to measure the strain in the main nib reinforcement and the hangers, such that the force in these bars were known at any time.

4.3 Experimental results

4.3.1 Shear resistance versus strut-and-tie models

As already explained, the nib result in a in a significant disturbance of the flow of the internal forces at the dapped-ends. Hence, the STM truss analogy is used to model the behaviour of the dapped-ends, in which struts represents the concrete compressive stress fields and ties normally represent one or several layers of reinforcement. However, the ties may also alternatively represent a concrete tensile stress field [18], i.e. the effect of fibres may be modelled by a tie which accounts for the bridging effect of the fibres through the residual tensile strength.

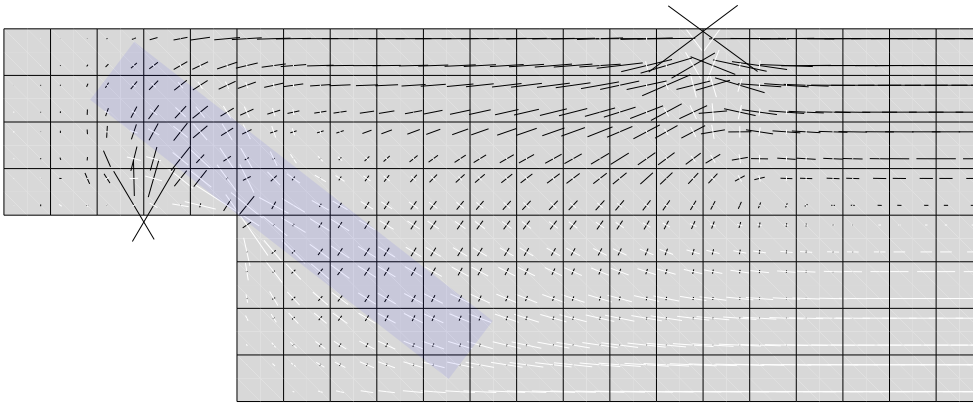

Figure 20: Close-up of the principal stress results from the elastic analysis in figure 13. The blue band represent the concrete tensile stress field which is effected through the residual tensile strength of the concrete.

In figure 20, a close-up of the flow of forces in the dapped-ends according to the elastic analysis in figure 13 is shown. From this, a fibre concrete tie at $\arctan(h/l) = 39°$ to the horizontal axis may be assumed. The thickness of the band may be taken as $h/(2H)$=0.25 of the length of the $(90 - 38.7) = 51.3°$ diagonal from the re-entrant corner to the top face of the beam. Hence, a model similar to that in figure 15 may be proposed, but with

the reinforcement tie replaced by a fibre concrete tie with inclination and thickness as specified above. The contribution of the fibres to the shear resistance may then be taken as the vertical component of the fibre concrete tie, in the same manner as in equation 22, which yields

$$V_f = b \cdot \overbrace{0.25 \cdot \frac{h}{\sin 51.3}}^{t_f} \cdot f_{ft,res,2.5} \cdot \sin 38.7 = 250 \cdot 0.25 \cdot \frac{200}{\sin 51.3} \cdot 4.0 \cdot \sin 38.7 = \underline{40.1\,kN} \tag{30}$$

Table 12 presents the calculated shear resistances of the various dapped-ends together with their measured counterparts. It can be seen that the SC-SFRC and SC-HFRC members exhibits similar behaviour even though they contain 1.0 vol% and 1.5 vol% fibres, respectively. This clearly demonstrates that the steel fibres are more effective than the synthetic fibres. Hence, for brevity, only the results for the SC-SFRC are considered in the following discussion.

Table 12: Main experimental parameters together with the measured shear resistance $V_{R,exp}$ and the estimated counterpart $V_{R,calc}$. The experimental resistance is the average of two results. V_s is the resistance provided by the conventional bar reinforcement according to equation 22 and 24, whereas V_f is the resistance due to fibres according to equation 30.

Batch nr.	Type of concrete	Reinf. layout	f_c (MPa)	$f_{ft,res,2.5}$ (MPa)	V_s (kN)	V_f (kN)	$V_{R,calc}$ (kN)	$V_{R,exp}$ (kN)	$\frac{V_{R,calc}}{V_{R,exp}}$
1	C40/50	A	43.2	0.0	144	0.0	144	262	0.55
1	C40/50	B	43.2	0.0	50.3	0.0	50.3	145	0.35
2	SC-SFRC	B	63.6	4.0	50.3	40.1	90.4	223	0.41
3	SC-HFRC	B	63.3	3.9	50.3	39.1	89.4	213	0.42
2	SC-SFRC	C	63.6	4.0	0.0	40.1	40.1	158	0.25
3	SC-HFRC	C	63.3	3.9	0.0	39.1	39.1	159	0.25
4	SC-SFRC	D	62.4	2.8	113	28.0	141	260	0.54
3	SC-HFRC	D	63.3	3.9	113	39.1	152	265	0.57

The effect of fibres. The increase in shear resistance due to fibres may be found by comparing the specimens of layout B. However, since the reference beam without fibres is made of a weaker concrete, its resistance must be adjusted for this. If the resistance is taken as $(63.6.0/43.2)^{1/3} = 1.14$ times the measured resistance, the strength gain due to fibres is $223/165 = 1.35$.

The effect of hangers. One vertical hanger and the inclined hangers are removed in layout B. Hence, if it is assumed that the horizontal stirrups and the beam shear reinforcement do not influence the results, the reference beam should be expected to carry $262 - 42.8 - 50.3 = 169\,kN$. This is $169/145 = 1.17$ times the actual resistance. Further, the only difference between layout B and C is one vertical hanger. Hence, layout C should be expected to carry $223 - 50.3 = 173\,kN$, which is 1.09 times the actual resistance. It should, however, be noted that the hangers in layout A, B and C all yielded at a load level equal to about 70 % of the shear resistance, i.e. they were subjected to a great deal of strain-hardening before failure. Their capacity based on the yield stress will

therefore tend to underestimate the hanger contribution. If this is accounted for, it can be claimed that the resistance of the dapped-ends are closely related to the amount of hanger reinforcement.

The effect of mid-centred-layout. If there is no beneficial effect of the mid-centred layout, the specimens of layout D is expected to carry $158 + 113 = 271\,kN$ (or more due to strain-hardening of the hangers). The measured resistance was actually lower than this. Hence, the 'optimised' layout seems to perform worse than a corresponding ordinary layout. The reason for this might be due to the fact that the force which is lifted up by the hanger is concentrated over a smaller area. The compressive zone then becomes more highly stressed, which might have caused a premature failure. Actually, Robinson et al. [16] have argued that the effective width of the concrete strut should be taken as that confined by the stirrups, i.e. the distance between the centreline of the reinforcement bars, and not the full width of the beam. This is supported by the fact that the collapse of the layout D beams was caused by failure of the concrete, and not the hangers as for the other layouts. Hence, although the mid-centred layout may be beneficial from a fibre point of view, it might in total come out worse due to a smaller effective width of the compressive struts.

The effect of the concrete. From table 12, it can be seen that the calculated resistances are very conservative, especially for the layouts containing a small amount of reinforcement. This is to be expected, since the concrete contribution is omitted in the calculations. According to the experiments, the concrete term can be estimated as $145 - 50.3 \cdot 1.10 = 90\,kN$ (if 10 % strain-hardening of the hanger is assumed) for the C40/50 concrete which corresponds to about $90 \cdot 1.14 = 103\,kN$ for the SC-SFRC. If this value is added to the calculations, the estimated values will match the experiments.

The shear force at cracking. Werner and Dilger [21] suggested that the shear force existing when cracking occurs at the re-entrant corner can be taken as the shear force which continues to be resisted by the concrete. The shear force was determined from an elastic finite-element analysis by taking the average of the stresses at the corners of the three elements which are connected at the re-entrant corner and comparing it to the tensile strength of the concrete. This procedure will of course be a bit arbitrary, since it depends on the mesh configuration. In figure 13, the mesh for a dapped beam of the same dimensions as the test specimens is shown. The size of the elements are $50 \times 50\,mm$, which are about three times the maximum size of the aggregate, i.e. about the size which is used to determine the tensile strength. If this configuration is utilised in the analysis and the tensile stress is taken as the average of the three integration points closest to the re-entrant corner, the shear force at cracking becomes $40\,kN$ (if the tensile strength is taken as $f_t = 0.30 \cdot 43.2^{2/3} = 3.69\,MPa$). This corresponds quite well to the shear force when the cracks were detected in the tests, which was typically around $50\,kN$. However, the concrete contribution according to the experiments is about twice this value. The reason for this is probably that the load is applied sufficiently close to the support to allow the concrete to carry a significant load after cracking by arch action.

The effect of the residual tensile strength. Although the residual tensile strength, as derived from the EN 14651 tests, is only $2.8\,MPa$ for the SC-SFRC beam of layout D, it does not seem to affect the experimental load-carrying capacity. The reason for this is

probably that the fibre orientation in this case was much more favourable in the structure compared to that of the EN 14651 tests.

4.3.2 Load-deflection behaviour

In figure 21, the load-deflection behaviour for the SC-SFRC members are compared to the reference beam. It can be seen that all SC-SFRC members exhibits rather ductile behaviour, but they are not quite as ductile as the reference beam. However, it is interesting to note that the SC-SFRC beams of layout C, i.e. the ones with no hanger reinforcement, do not suffer a brittle failure but exhibits a gradual decay of load-carrying capacity. This means that it may be possible to skip the hanger reinforcement in lightly loaded dapped-end RC beams if they are made of ductile fibre-reinforced concrete.

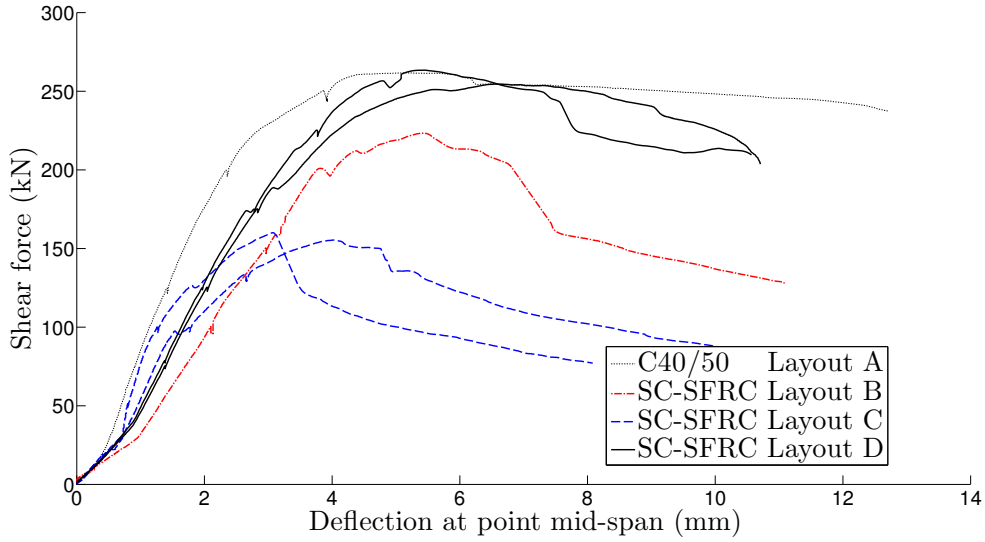

Figure 21: Shear force versus deflection at mid-span for the SC-SFRC members compared to the reference beam. Only the results for one of the dapped ends are shown for layout A and B due to to errors in testing.

Further, it can be seen that by adding one ø8 hanger to layout C (which gives layout B) the shear resistance goes up by $65\,kN$, which is a little more than the capacity of the hanger. However, if a mid-centered ø12 hanger is added to layout C (which gives layout D if the remaining reinforcement is also mid-centred), the capacity goes up by $102\,kN$, which is a little less than the capacity of the hanger. It therefore seems that the mid-centred layout is unfavourable when it comes to shear resistance, as already mentioned in the previous section. The ductility, on the other hand, seems to be enhanced.

4.4 Conclusions

The behaviour of the SC-SFRC and SC-HFRC members was similar even though the former contained 1.0 vol% steel fibres and the latter contained 1.5 vol% steel and synthetic fibres in a 50/50 mix. This clearly demonstrates that the steel fibres are more effective

than the synthetic fibres, which is maybe not that surprising, since it is well-known that steel fibres are to be preferred when it comes to shear-resistance.

The strength gain due to fibres was about $50\,kN$, which corresponds to that of a ø8 vertical stirrup used as hanger reinforcement. Hence, the potential benefits of fibres lies not so much in its contribution to the strength, but is more related to the possibility of removing secondary reinforcement and the beam shear reinforcement, which might lead to a much less labour-intensive production of the precast elements.

The estimated shear resistance of the dapped-ends was almost directly related to the capacity of the hanger reinforcement. This indicates that the strut-and-tie models used in the calculations are adequate. The deviations between the experimental and calculated values were therefore believed to be partly due to the neglect of the strain-hardening of the steel bars, but foremost a result of the neglect of the concrete contribution to the shear resistance.

Another important observation was that the mid-centred reinforcement layout, which was expected to be very favourable, actually performed worse than expected for an ordinary layout. This might have been due to the fact that a mid-centred layout tend to concentrate the force which are lifted up by the hanger, which might have caused a premature failure of the compressive struts.

It is also interesting to note that the fibre-reinforced dapped-end without hanger reinforcement did not suffer a brittle failure. This means that it may be possible to skip the hanger reinforcement in lightly loaded dapped-end RC beams if they are made of ductile fibre-reinforced concrete.

The proposed strut-and-tie model, which accounts for the effect of fibres, led to good predictions for the dapped-ends in the tests. This is maybe not so impressive, since it merely could have been 'tuned' to fit the rather limited amount of data in the test program. Hence, in order to evaluate the the tentative model presented herein, more experimental data is needed. This is the subject of a future article.

References

[1] www.coinweb.no.

[2] T. Kanstad et al. Forslag til retningslinjer for dimensjonering, utførelse og kontroll av fiberarmerte konstruksjoner (in norwegian). COIN Project report 29, 2011.

[3] O. S. Nordhus, E. Steinnes, and T. Simpson. Fibre reinforced concrete structure: Use of self compacting ductile fibre reinforced concrete in beams and slabs (in norwegian). Master's thesis, Norwegian University of Science and Technology, 2011.

[4] T. Backe-Hansen and B. Hamstad. Fibre reinforced concrete structures: Testing of prefabricated beams with dapped beam end (in norwegian). Master's thesis, Norwegian University of Science and Technology, 2011.

[5] H. Vikan. Concrete workability and fibre content. SINTEF report, SBF BK A07029, 2007.

[6] NS-EN 1992-1-1:2004+NA:2008. Eurocode 2: Design of concrete structures. part 1-1: General rules and rules for buildings. Standard Norge, 2008.

[7] NS-EN 14651:2005+A1:2007. Test method for metallic fibre concrete. Standard Norge, 2007.

[8] D. Hordijk. *Local approach to fatigue of concrete*. PhD thesis, Delft University of Technology, 1991.

[9] Å. L. Døssland. *Fibre reinforcement in load carrying concrete strutures*. PhD thesis, Norwegian University of Science and Technology, 2008.

[10] W-Y Lu, I-J Lin, S-J Hwang, and Y-H Lin. Shear strength of high-strength concrete dapped-end beams. *Journal of the Chinese Institute of Engineers*, 26(5):671–680, 2003.

[11] A.H. Mattock and T.C. Chan. Design and behavior of dapped-end beams. *PCI Journal*, 24(6):28–45, 1979.

[12] A.H. Mattock and T.S. Theryo. Strength of precast prestressed concrete members with dapped ends. PCISFRAD Project No. 6, 1986.

[13] J.M. Ajina. Effect of steel fibers on precast dapped-end beam connections. Master's thesis, South Dakota State University, 1986.

[14] Z. Fu. Use of fibre and headed bars in dapped end beams. Master's thesis, McGill University, 2004.

[15] R.N. Mohamed and K.S. Elliott. Shear strength of short recess precast dapped end beams made of steel fibre self-compacting concrete. 33rd Conference on OUR WORLD IN CONCRETE & STRUCTURES: 25-27 August, 2008.

[16] G.P. Robinson, A. Palermi, and S.A. Austin. Influence of steel fibre, used in conjuction with unconfined rebar configurations, on the structural performance of precast elements. BEFIB 2012 - Fibre reinforced concrete, 2012.

[17] *Betongelementboken - Bind C: Elementer og knutepunkter*. Betongelementforeningen, 2006.

[18] J. Schlaich and K. Schäfer. Design and detailing of structural concrete using strut-and-tie models. *The structural engineer*, 69(6):113–125, 1991.

[19] A.H. Mattock. Strut-and-tie models for dapped-end beams. *Concrete International*, pages 35–40, February 2012.

[20] A. Steinle and F.S. Rostasy. Zum tragverhalten ausgeklinkter trägerenden. *Betonwerk Fertigteil-Technik*, 41(6/7), 1975.

[21] M.P. Werner and W.H. Dilger. Shear design od prestressed concrete stepped beams. *PCI Journal*, 18(4):37–49, 1973.

Appendix A MatLab Code for multi-layer analysis

```
function [f,m,slam,slam1,x,curv] = multilayer(ebot,etop)

% ------------------------------------------------------
% H. Nedrelid 02.06.2013
% ------------------ INPUT -----------------------------
% fc      = concrete cylinder strength
% fres    = concrete residual tensile strength
% Es      = Youngs modulus of steel bars
% fy      = yield stress of steel bars
% nlam    = number of layeres
% b       = width of cross-section
% h       = height of cross-section
% c1      = cover to tensile bars
% c2      = cover to compressive bars
% n1      = number of tensile bars
% n2      = number of compressive bars
% ------------------ OUTPUT ----------------------------
% f       = axial force
% m       = moment
% slam    = stress in concrete layers
% slam1   = stress in tensile bars
% x       = compressive depth of concrete
% curv    = curvature
% ------------------------------------------------------

multilayerinput

% CONCRETE PROPERTIES
if fc <= 50
    ft = 0.30*(fc)^(2/3);
elseif fc > 50
    ft = 2.12*log(1+(fc/10));
end
Ec = (22*((fc)/10)^0.3)*1000;
if fc <= 50
    ec2  = -2.0/1000;
    ecu2 = -3.5/1000;
    n    = 2.0;
elseif fc > 50
    ec2  = -(2.0+0.085*(fc-50)^(0.53))/1000;
    ecu2 = -(2.6+35*((90-fc)/100)^4)/1000;
    n    = 1.4+23.4*((90-fc)/100)^4;
end
if fres > ft
    ft = fres;
end

% REINFORCEMENT PROPERTIES
As1 = n1*pi*(d1/2)^2;
As2 = n2*pi*(d2/2)^2;

% INITIAL CALCULATIONS
d = h-c1-d1/2;
h1 = h-d;
if n2>0
    h2 = c2+n2/2;
else
    h2 = 0;
end
curv = (ebot-etop)/h;
if curv == 0
    x = 0;
else
    x  = (abs(etop)*h)/(ebot-etop);
end

```

```
67  % INTERNAL LEVEL ARMS FOR CONCRETE LAYERS
68  hlam = h/nlam;
69  href(1,1) = hlam/2;
70  for i = 2:nlam
71      href(i,1) = href(i-1,1)+hlam;
72  end
73  for i = 1:nlam
74      hrefy(i,1) = href(i,1)-h/2;
75  end
76
77  % LAYER STRAINS, STRESSES, FORCES AND MOMENTS
78  for i = 1:nlam
79      elam(i,1) = curv*((h-href(i,1))-x);
80      if elam(i,1) <= ec2
81          slam(i,1) = -fc;
82      elseif elam(i,1) > ec2 && elam(i,1) <= 0
83          slam(i,1) = -fc*(1-(1-elam(i,1)/ec2)^n);
84      elseif elam(i,1) >= (ft/Ec)
85          slam(i,1) = fres;
86      elseif elam(i,1) < (ft/Ec) && elam(i,1) >= 0
87          slam(i,1) = elam(i,1)*Ec;
88      end
89      flam(i,1) = slam(i,1)*b*hlam;
90      mlam(i,1) = flam(i,1)*hrefy(i,1);
91  end
92
93  % INTERNAL LEVEL ARMS FOR THE REINFORCEMENT
94  href1 = h1;
95  href2 = h-h2;
96  hrefy1 = h1-(h/2);
97  hrefy2 = href2-(h/2);
98
99  % REINFORCEMENT STRESSES
100 elam1 = curv*((h-href1)-x);
101 if abs(elam1) >= 0 && abs(elam1) <= fy/Es
102     slam1 = elam1*Es;
103 elseif abs(elam1) > fy/Es && elam1 < 0
104     slam1 = -fy;
105 elseif abs(elam1) > fy/Es && elam1 > 0
106     slam1 = fy;
107 end
108 elam2 = curv*((h-href2)-x);
109 if abs(elam2) >= 0 && abs(elam2) <= fy/Es
110     slam2 = elam2*Es;
111 elseif abs(elam2) > fy/Es && elam2 < 0
112     slam2 = -fy;
113 elseif abs(elam2) > fy/Es && elam2 > 0
114     slam2 = fy;
115 end
116
117 % REINFORCEMENT FORCES AND MOMENTS
118 flam1 = slam1*As1;
119 flam2 = slam2*As2;
120 mlam1 = flam1*hrefy1;
121 mlam2 = flam2*hrefy2;
122
123 % RESULTANTS
124 f = sum(flam) + flam1 + flam2;
125 m = sum(mlam) + mlam1 + mlam2;
126
127 format short
128 f = f*10^-3;
129 m = m*10^-6;
130
131 end
```

```
function [moment,curvature,epst,epsc,sigt,sigc,ad,sigs] = multilayerloop()

% -- OUTPUT FOR EACH STEP COLLECTED IN VECTORS--
% moment    = moment
% curvature = curvature
% epst      = concrete strain in bottom layer
% epsc      = concrete strain in top layer
% sigt      = concrete stress in bottom layer
% sigc      = concrete stress in top layer
% ad        = compressive depth of concrete
% sigs      = stress in flexural bars
% ------------------------------------------

multilayerinput

i = 0;
m = 0;
curv = 0;
etop = 0;
slam(1:nlam,1) = zeros;
x = 0;
slam1 = 0;
lim = 3/h;
for ebot = 0:0.00001:lim
    i = i+1;
    f = 9999999;
    moment(i,1)    = m;
    curvature(i,1) = curv;
    epst(i,1)      = ebot;
    epsc(i,1)      = etop;
    sigt(i,1)      = slam(1,1);
    sigc(i,1)      = slam(nlam,1);
    ad(i,1)        = x;
    sigs(i,1)      = slam1;
    elamp = etop;
    for etop = elamp:-0.000001:-0.02
        [f,m,slam,slam1,x,curv] = multilayer(ebot,etop);
        if f < 0.01
            break
        end
    end
    %if abs(moment(i,1)) > 0.60*54.5
    %  break
    %end
end
plot(cu,abs(mm),'--k','linewidth',1.8)

end
```

SINTEF Building and Infrastructure is the third largest building research institute in Europe. Our objective is to promote environmentally friendly, cost-effective products and solutions within the built environment. SINTEF Building and Infrastructure is Norway's leading provider of research-based knowledge to the construction sector. Through our activity in research and development, we have established a unique platform for disseminating knowledge throughout a large part of the construction industry.

COIN – Concrete Innovation Center is a Center for Research based Innovation (CRI) initiated by the Research Council of Norway. The vision of COIN is creation of more attractive concrete buildings and constructions. The primary goal is to fulfill this vision by bringing the development a major leap forward by long-term research in close alliances with the industry regarding advanced materials, efficient construction techniques and new design concepts combined with more environmentally friendly material production.